Expression of Interest for Nuclear/Hadron Physics Experiments at the 50-GeV Proton Synchrotron

M. Asakawa[1], J. Chiba[2], H. En'yo[3], G. T. Garvey[11], H. Hamagaki[4], O. Hashimoto[5], T. Hatsuda[6], M. Ieiri[2], T. Kishimoto[7], Y. Miake[8], J. M. Moss[11], T. Murakami[3], K. Nakazawa[9], A. Ohnishi[10], K. Ozawa[4], J. C. Peng[11], S. Sawada[2], M. Sekimoto[2], T. -A. Shibata[12], T. Sugitate[13], H. Tamura[5], K. H. Tanaka[2] and S. Yokkaichi[14]

[1] *Department of Physics, Nagoya University, Nagoya 464-8602, Japan*
[2] *Institute of Particle and Nuclear Studies, High Energy Accelerator Research Organization, Ibaraki 305-0801, Japan*
[3] *Department of Physics, Kyoto University, Kyoto 606-8502, Japan*
[4] *Center for Nuclear Study, University of Tokyo, Tokyo 113-0033, Japan*
[5] *Department of Physics, Tohoku University, Miyagi 980-8578, Japan*
[6] *Department of Physics, University of Tokyo, Tokyo 113-0033, Japan*
[7] *Department of Physics, Osaka University, Osaka 560-0043, Japan*
[8] *Institute of Physics, University of Tsukuba, Ibaraki 305-8571, Japan*
[9] *Physics Department, Gifu University, Gifu 501-1193, Japan*
[10] *Department of Physics, Hokkaido University, Hokkaido 060-0808, Japan*
[11] *Physics Division, LANL, Los Alamos, NM 87545, USA*
[12] *Department of Physics, Tokyo Institute of Technology, Tokyo 152-8551, Japan*
[13] *Department of Physics, Hiroshima University, Hiroshima 739-8526, Japan*
[14] *RIKEN (Institute of Physical and Chemical Research), Saitama 351-0198, Japan*

Abstract

Intention is expressed to pursue the physics of strongly interacting many-body systems at the planned 50-GeV Proton Synchrotron of the KEK/JHF and JAERI/NSP joint accelerator project. The richness of the field is emphasized and several possible experiments are discussed. In order to carry out these experiments, a multipurpose beam line is proposed which can transport protons, heavy ions, pions and other secondary particles of various energy with intensities from 10^9 to 10^{12} pps.

Contents

Chapter 1

Introduction

1.1 Motivation

The Japan Hadron Facility (JHF) project at the High Energy Accelerator Research Organization (KEK), which was originally proposed by scientists of nuclear physics and other fields, has been merged with the Neutron Science Project (NSP) of Japan Atomic Energy Research Institute (JAERI), and has become a joint project. The joint project has not been officially approved yet by the Japanese government, but people are working towards its formal approval in the near future. We think that it is very important to express our interest at a timely opportunity when the construction plans are being discussed seriously, even though there is no official call for letters of intent by the project office.

In this article, we would like to express our interest in physics experiments on nuclear/hadron physics using the 50-GeV proton synchrotron (50-GeV PS). We have discussed possible physics at the 50-GeV PS through workshops and conferences. Among various nuclear/hadron physics topics discussed, we have found that a set of them, which was called "physics with primary beams" before, could be investigated experimentally with a beam line which can produce not only proton beams, but also secondary beams, as described later in this article.

1.2 Richness of hadron physics at 50-GeV PS

"Desire to explore the ultimate form of matter": this has motivated human beings to study philosophy, sciences and technologies, a part of which blossomed later, throughout our history.

The accelerators at the high-energy frontier, such as the Large Hadron Collider (LHC) or the Linear Collider, aim to discover ultimately small particles (= elementary particles). High-energy lepton accelerators, such as the Jefferson Laboratory or the SPring-8, look at ultimately small regions of matter. The purpose of the Relativistic Heavy Ion Collider (RHIC) is to create an ultimately hot state of matter or a quark-gluon plasma (QGP), which corresponds to the state at the beginning of our universe.

The major motivation of the 50-GeV PS facility is to investigate ultimately dense and heavy matter, that is, nuclear matter. The heaviest nuclei in the universe are neutron stars, except for black holes. In nuclear matter, the interaction is so strong that hadrons cannot be the same as they are in free space; then/and/or new particle degrees of freedom can emerge. For example, inside a neutron star where *cold and dense nuclear matter* is formed, various states of matter have been theoretically speculated, such as pion condensation, kaon condensation, hyperon matter, and quark matter. Even in normal nuclei, which are *already very dense*, it is strongly suggested that the properties of strongly interacting particles, such as vector mesons, would be different from those in free space. In high-energy heavy-ion collisions, where *hot,*

dense nuclear matter is expected to be formed, most of the interaction energy is converted into hydrodynamical radial flow energy after the highest density is reached. In order to understand nuclear matter, including these states and phenomena, we have to investigate various properties of nuclear matter in a variety of states as much as possible as well as the fundamental principle of the strong interaction, quantum chromodynamics (QCD).

At the 50-GeV PS, nuclear matter is studied from various points of view. In the following two sections, some examples are briefly reviewed.

1.2.1 Physics with pA reactions

The fundamental theory of strong interaction is QCD. Nuclei and nuclear matter are, in principle, described by QCD. QCD is a non-Abelian gauge theory, in which the gauge boson interacts with itself, and is asymptotically free at high energies. On the other hand, the gauge coupling constant in QCD increases as the energy scale decreases [1, 2], which invalidates the perturbative expansion in low-energy regions. Partly because of this, nuclear physics has been studied largely by means of effective theories/models. Not many of them have respected the underlying symmetries in QCD. Also, not many of them have been based on the solid ground of the general principles of QCD. We intend to carry out research to reveal various aspects of quantum chromo many-body dynamics.

Elementary excitation in nuclear matter In modern solid state physics, or "quantum electro many-body physics", the first things to be studied are elementary excitations in matter [3], their change as a function of temperature, pressure,...etc., and the interactions with each other, and so on. Then, phase transition is often understood in terms of elementary excitations or effective degrees of freedom. In nuclear physics, however, a consensus has not yet been reached about the effective degrees of freedom in matter.

Nuclei are the only laboratory which is practically available with sufficiently high and known density and with a uniformity sufficient to measure excitations in strongly interacting matter, such as the ω meson, ϕ meson, and so on. Obtaining information on elementary excitations in nuclear matter will deepen our understanding of QCD as a quantum field theory in the non-perturbative region, and should take it far beyond understanding by such somewhat classical concepts as the mean potential, effective mass,...etc. [4, 5]. To measure the vector spectral function in nuclei through dilepton decays of vector mesons will provide invaluable clues to such information [6, 7].

Unlike in the case of QED, elementary excitations in QCD are composite, even in the vacuum. Hadrons are made of more fundamental particles/fields, i.e., partons, or quarks and gluons. One way to characterize the quantum state of partons in hadrons is through the structure functions. As discussed in a later chapter, the structure functions in nuclei are known to be modified. Considering the fact that electrons in matter are different from those in the vacuum due to quantum dressing, which is well-known in solid state physics, this itself is not an unexpected phenomenon. The electron states in the solid state have been continuously showing their diverse possibility. QCD is expected to allow much richer physics thanks to the existence of self-couplings among the gauge bosons, gluons. A modification of the structure functions in nuclei should provide deeper information on QCD in intermediate energy regions than mere trivial effects, such as the Fermi motion effect.

Energy loss in QCD The energy loss of partons traversing a quark-gluon plasma exemplifies the importance of gluon self-couplings in QCD. In QED, it has been known that to understand a similar problem, the energy loss of electrons traversing a dense electron plasma, it is essential to take account of quantum interference; because of quantum interference, the radiative energy

loss is suppressed at high density (Landau-Pomeranchuk effect) [53, 9]. In QCD, however, destructive interference is incomplete because of an additional graph that includes gluon self-coupling. Furthermore, it has been shown in perturbative QCD that final-state interaction of radiated gluons, which is again due to self-coupling, is crucial for a radiative energy loss. As a result, the energy loss becomes non-local, i.e., it depends on the size of the system [10, 11, 12, 13, 14], while in the QED case it is local and the energy loss per trajectory length is constant.

These are only a part of the examples that show the richness of quantum chromo many-body physics. It cannot be emphasized too much that nuclei are the only possible laboratory to explore such diverse possibilities in a static condition with known density. pA physics is complementary with e^-A and γA physics from this point of view.

1.2.2 Physics with nuclear collisions

The 50-GeV PS is an ideal place to explore high-density QCD matter. As explained in a later chapter, it is now experimentally established that the highest possible baryon density accessible by nuclear collisions is achieved at some energy between the AGS (11.6 GeV/A) and SPS (160 GeV/A) energies [15, 16]. It will also be important to note here that the heaviest possible nuclei (such as Au and U) are not necessary to produce high-density matter, though they are preferred. The significance of exploring the high baryon density region is many fold. The following only gives examples of motivations for studying high baryon density matter.

First, it is the region where a lattice QCD simulation cannot yet be carried out. This is a technical and at the same time conceptual problem [17]. The complete solution to this problem has not been found. Thus, this region cannot be accessed non-perturbatively with only first principles. Quite often, this region is studied with effective models. However, there is no guarantee that models that reproduce nuclear matter properties can also predict the properties of very high-density matter at finite temperature. A consistent perturbative expansion scheme in relativistic finite-temperature field theory was found only in the 90's [18]. Furthermore, the perturbative expansion for the thermodynamical potential in QCD at finite temperature is known to break down beyond $O(g^6)$ [19], where g is the QCD coupling constant. We do not have much reliable information on the properties of hot and dense QCD matter (in hadron or QGP phase). It is thus quite significant to explore the $T-\mu$ plane as extensively as possible.

Second, many possibilities have been proposed for regions at high baryon density and comparatively low temperature: pion condensation, kaon condensation, hyperon matter, color superconductivity, and so on. The region explored by 50-GeV PS is expected to be in between the T axis and such regions on the $T-\mu$ plane. The data obtained at 50-GeV PS will contribute to the understanding of such phases, although none of them is expected to actually be created.

Finally, we present in the following an excerpt from Gross, Pisarski, and Yaffe's article [20], which was written 20 years ago. We believe that this is still truth.

...Presented with a new theory involving novel and unfamiliar physical mechanisms, it is of great value to explore its properties in as wide a set of circumstances as possible. It is particularly important to try to extend the theory to explain phenomena which are far removed from the observations that originally motivated the theory. This effort can test the consistency and reasonableness of the theory, increase confidence in its predictive power, and deepen one's understanding of its structure...

—— Gross, Pisarski, and Yaffe

1.3 Overview of our intention

As emphasized in the previous sections, one of the most important themes in nuclear physics is the study of nuclear matter. We would like to start with experiments using 50-GeV proton beams or particle beams from 50-GeV proton beams to study nuclear matter and QCD. When heavy-ion beams and/or polarized proton beams become available, research in this field will become much more versatile and prolific.

In this article, we would like to present physics contents in some detail in Chapter 2. Section 2.1 describes the study of the chiral property of nuclear matter with light vector mesons. Section 2.2 is for the study of a relatively high mass region of lepton pairs, such as J/ψ production or the Drell-Yan process. Section 2.2 also includes possible research themes with polarized proton beams in the future. Section 2.3 deals with multifragmentation. Section 2.4 describes possible experiments for strangeness physics with single- or multi-strangeness projectile fragments, which will be available when heavy-ion beams are accelerated in the future. Section 2.5 gives a description of hadron measurements with heavy-ion beams. Section 2.6 describes possible experiments with future polarized beams and/or targets.

Of course, nuclear physics has multiple aspects and there are many other research subjects which can be made possible with high-energy particle beams from the 50-GeV PS. Hadron spectroscopy is used to study exotic states of nucleons and mesons, which lead to our deeper understanding of the strong interaction. With an antiproton beam from the 50-GeV PS, charmed nuclei can be produced. Japanese scientists have been leading the field of strangeness nuclear physics, which intends to understand baryons and nuclei in the SU(3) octet. The study of charmed nuclei, for example, nuclei with one nucleon replaced by Λ_c^+, will shed light on the SU(4) aspects of the baryon interaction. These subjects will be discussed in another article in the future.

Chapter 3 describes the proposed beam line and our interest is summarized in Chapter 4.

Chapter 2

Experiments

2.1 Study of the chiral property of dense nuclear matter through measurements of the meson-spectral-change in medium

2.1.1 Introduction

In QCD, quarks and gluons are confined inside color singlet hadrons. Furthermore, the dynamical breaking of chiral symmetry in the QCD vaccum induces an effective mass of quarks, which has been known phenomenologically as "constituent quark mass". The quark condensate $\langle\bar{q}q\rangle$, which takes $-(225\pm 25)$ MeV^3 in the vacuum, is an order parameter of this dynamical breaking of chiral symmetry.

Numerical simulations in lattice QCD as well as model calculations show that $\langle\bar{q}q\rangle$ is subject to change in hot (T$\neq$ 0) and/or dense ($\rho \neq 0$) matter where chiral symmetry is restored or partially restored. Although $\langle\bar{q}q\rangle$ is not a direct experimental observable, the spectral changes of mesons and baryons may provide a good measure of such partial retoration of chiral symmetry and associated change of $\langle\bar{q}q\rangle$ (see the reviews, [21, 22]). Experimental observation of in-medium modifications of mesons is thus highly desirable to study the nature of QCD in the non-perturbative region.

Among other mesons, the neutral vector mesons are unique for studing spectral changes, since they can decay into dileptons which do not suffer from strong interactions, and thus carry information of the meson properties in matter. In fact, the observed excess of low-mass dileptons by the CERN heavy-ion experiments may already hint a precursor of the symmetry restoration in hot and dense hadronic matter [24].

On the other hand, in cold nuclear matter, a linear decrease of $\langle\bar{q}q\rangle$ is expected at low densities. This may also be reflected in the spectral changes of the ρ, ω and ϕ mesons, which has attracted considerable theoretical studies (see [25, 26, 27, 28] for early references and see the papers in [29] for recent developments.) In Figure 2.1, one of such calculations based on the in-medium QCD sum rules [25] is shown. Based on the QCD sum rule, according to this approach, the mass decrease of ω is 140 MeV and ϕ in the range of 20 to 40 MeV at normal nuclear density ρ_0.

Several experimental efforts have been started to investigate the in-medium properties of the vector mesons at normal nuclear-matter density.

Table 2.1 lists those experiments. Due to many apparent reasons, such a nuclear matter effect is best measured through leptonic decay modes. Up to now, only 2 experiments are being performed. The results of experiment E325 will be described in the next section.

Experimentally, a detection of ϕ mesons at rest is nearly impossible since the daughter kaons decay immediately. Nevertheless with slower ϕ mesons, a larger decay probability inside a nucleus and a lager nuclear matter effect is expected to be observed.

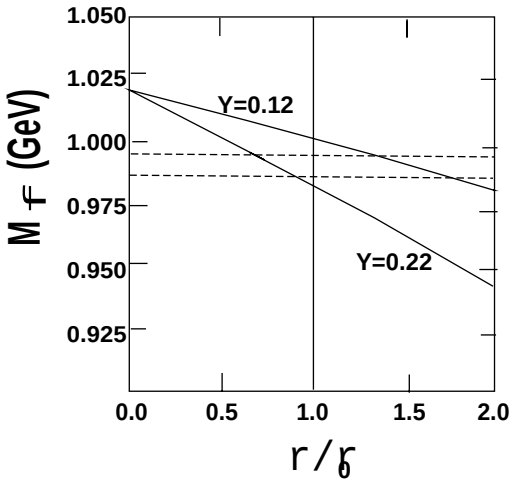

Figure 2.1: QCD sum-rule predictions for the density dependence of the mass of ϕ meson. The dashed lines are the threshold of the $K\bar{K}$ channels. The two solid lines represent the range of the strange-quark condensate expected from the experimental observation (Y=$2\langle s\bar{s}\rangle/(\langle u\bar{u}\rangle + \langle d\bar{d}\rangle)$).

Table 2.1: Experiments to study the nuclear density effect on vector mesons

place	channel	status	Ref.
KEK(Tanashi)-ES	$\gamma + A \to \rho + X$ $(\rho \to \pi^+\pi^-)$	Published	[70]
KEK-PS	$p + A \to \phi + X(\phi \to K^+K^-/e^+e^-)$	Running (E325)	[31]
SPring-8	$\gamma + A \to \phi + X$ $(\phi \to K^+K^-)$	Ready to run	[32]
GSI/HADES	$\pi + A \to \omega + X$ $(\omega \to e^+e^-)$	Preparation	[33]
GSI/FRS	$d + A \to^3 He + A^*$(bound)	Ready to run	[34]

It should be noted that the production of vector mesons with a nuclear target has not been well studied so far. The cross section of particle productions with a nuclear target normally follows the relation of $\sigma(A) = \sigma(1) \times A^\alpha$, where A is the nuclear mass number. In the production of J/ψ and the Drell–Yan lepton–pairs, α is close to unity at high energy, as measured in $\mu^+\mu^-$ pairs by Binkley *et al.* in 300-GeV/c $n + A$ interaction[35]. To produce those particles requires partonic interactions, like $g + g \to J/\psi + g$ or $q + \bar{q} \to \gamma^*$, i.e. the production is supposed to be perturbative and all of the nucleons in a nucleus contribute equally to the production. In the production of π, ρ and ω mesons, α is almost 2/3, which corresponds to the projective surface area of the nucleus. Those particles, consisting of light $u(\bar{u})$ and $d(\bar{d})$ quarks, are produced during fragmentation, and the yield is supposed to be governed by the first collision of an incident proton whose mean free path in the nucleus is much shorter than a typical nuclear radius. Regarding the production of the ϕ meson, Binkley *et al.* showed α to be 0.66 ± 0.03, close to 2/3, although their identification of the ϕ meson was not perfect, due to the poor mass resolution. Bailey *et al.* measured the mass-number dependence of the ϕ production in the K^+K^- channel in 120-GeV/c $p + A$ interaction and obtained $\alpha = 0.86 \pm 0.02$ [36]. Aleev *et al.* measured $\phi \to K^+K^-$ decays in 70-GeV $n + A$ interaction and obtained $\alpha = 0.81 \pm 0.06$ [37]. All of the ϕ productions mentioned above were measured in the kinematical region $0 \leq x_F \leq 0.3$ and $0 \leq p_T \leq 1$ GeV/c. No measurement of the target mass dependence of the ϕ meson production had been performed in the region of $x_F \leq 0$, close to the target rapidity.

Thus simultaneous measurements in the mesonic decay mode and the leptonic decay mode are very important to explore this field of physics.

Experiment E325

The experiment is located at the primary beam line of the KEK 12-GeV Proton Synchrotron. Special emphases are put on the detection of slowly moving ϕ mesons ($\beta\gamma_{lab} \leq 2$), which have a larger probability to decay inside nucleus, and simultaneous measurements of the $\phi \to K^+K^-$ and $\phi \to e^+e^-$ decays in the same apparatus. Apparently, the spectrometer can also detect $\omega/\rho \to e^+e^-$ decays. It should be noted that a high-quality primary beam on thin targets is needed to suppress the background from γ-conversion in the e^+e^- channel.

Until now, E325 has reported the data of $\phi \to K^+K^-$ decays and $\omega \to e^+e^-$ decays in the 12-GeV $p + A$ interaction.

Figures 2.2 and 2.3 show schematic layouts of the experiment. Beam protons were delivered to three targets (typically carbon, copper and polyethylene) placed in-line at the center of the spectrometer magnet.

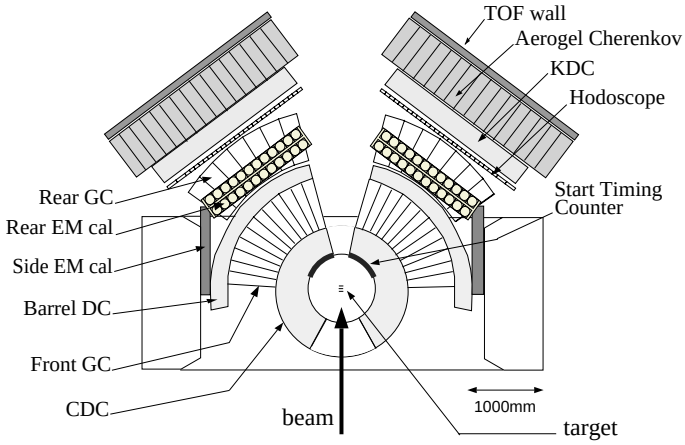

Figure 2.2: Top view of the E325 setup

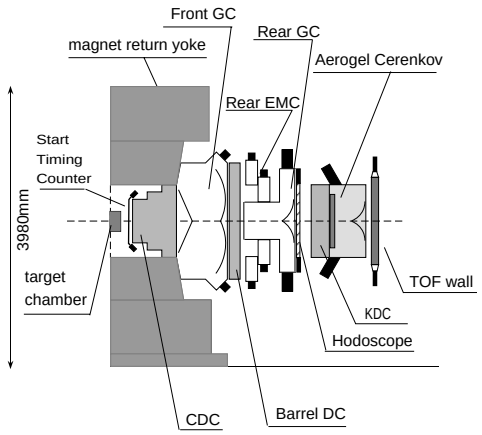

Figure 2.3: Side view of the E325 setup

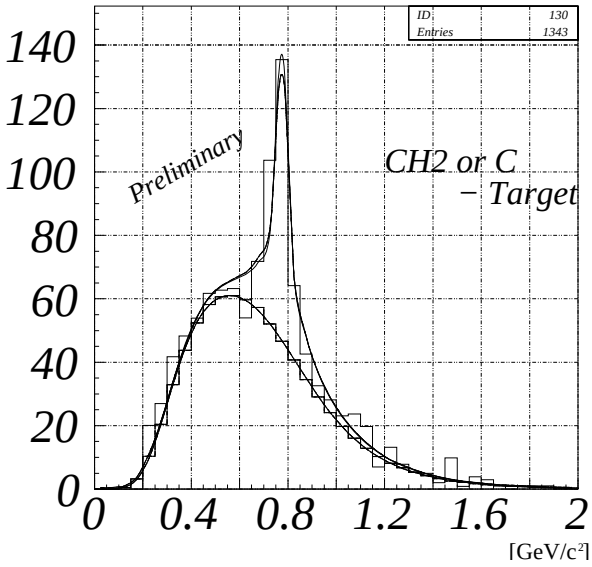

Figure 2.4: Electron-pair spectrum from a carbon target. The curves are the fit of ρ, ω resonances together with a mixed-event background.

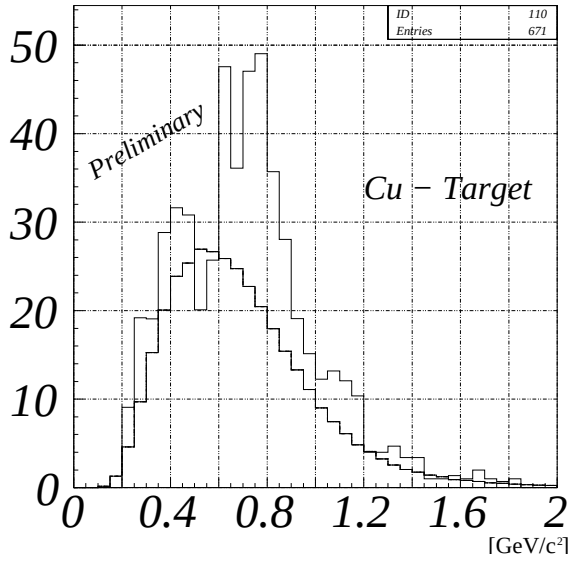

Figure 2.5: Electron-pair spectrum from a copper target. The this curve is a background shape estimated with a mixed-event method.

The spectrometer has two arms for kaon and electron detection, sharing the magnet and the tracking devices as being common. The kaon arms cover from $\pm 12°$ to $\pm 54°$ horizontally and $\pm 6°$ vertically, where the horizontal angle was measured from the beam line and the vertical angle was measured from the horizontal plane. The electron arms have a much larger acceptance, covering from $\pm 12°$ to $\pm 90°$ horizontally and $\pm 22°$ vertically.

The obtained invariant mass spectra of the e^+e^- pairs are shown in Figures 2.4 and 2.5 for carbon and copper targets. A clear peak of the ω meson is observed in the carbon target data. A difference between the two nuclei is visible. The broader peak (or can be double peaks) in the copper target data can be the signal of a nuclear matter modification on ω. The width is rather consistent with a prediction by Hatsuda.

E325 also reported the spectrum of the K^+K^- decay mode. A possible resonance-shape modification on the mesonic channel has yet to be worked out. The mass-number dependence of the production of the ϕ meson is reported using the standard parametrization, $\sigma(A) = \sigma(A = 1) \times A^{\alpha}$, where A is the atomic mass number of the target nucleus. The results are plotted in Figure 2.6 together with the best fit line.

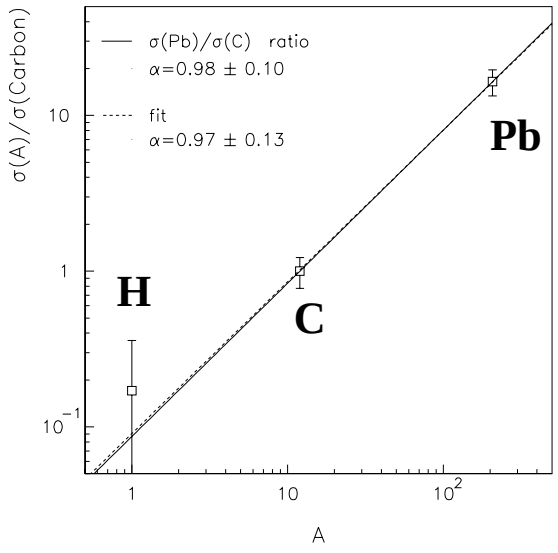

Figure 2.6: Mass-number dependence of the cross section. The solid line is obtained by the ratio of the lead to the carbon data. The dashed line is the best fit over the three points. The data point for hydrogen is obtained by the CH_2–C subtraction.

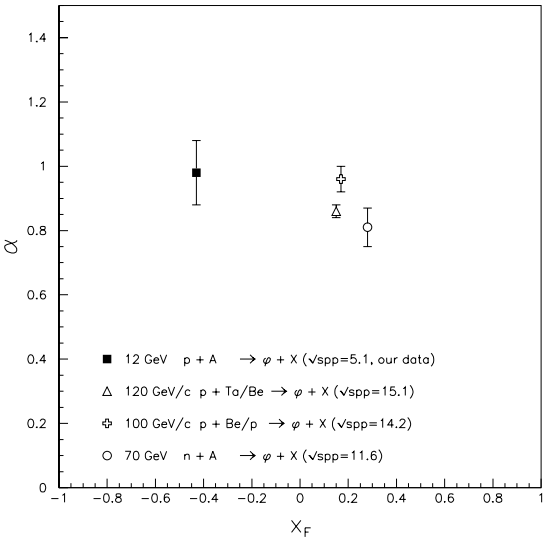

Figure 2.7: x_F dependence of the α parameter

The obtained α parameter is plotted in Figure 2.7 together with other available data[36, 37] as a function of the x_F of the observed ϕ mesons. In spite of the large difference in incident energies and in the kinematical coverages, the obtained α is consistent with those of other experiments.

The fact that the α parameter is close to unity at this energy region ($\sqrt{s}$ = 5.1 GeV) is surprising. It is generally believed that the incident energy of 12 GeV is dissipated rapidly and the nucleons in the back half of the nucleus can not contributed to the particle production. The present results suggest that the production mechanism of ϕ mesons is similar to that of J/ψ at higher energy, which is visible because the production from the fragmentation is largely suppressed due to the significant heavy mass of the $s\bar{s}$ and OZI suppression.

This experiment is the first attempt to measure the production and decay of vector mesons in the kinematical region where the effect of nuclear media should play an important role. The surprising feature observed in the e^+e^- spectrum should be further studied in the 50-GeV accelerator.

2.1.2 Experiments at the 50-GeV Proton Synchrotron

Although the experiment at the 50-GeV PS is philosophically an extension of the present PS-E325 experiment, we would like to propose significant qualitative improvements both in the beam line and in the spectrometer.

Requirement on the beams and the beam line

We would like to request a primary beam of 10^9/sec with a beam spot size of a few hundred of microns. Such a pencil beam was once achieved at the H8 beam line at CERN SPS. At H8, $25\mu m$ (base width) beam spot with the intensity of 10^6/sec was stably provided with 450-GeV primary protons. The merits of such a well-defined beam are many. We can expect a smaller halo around the beam, so that counter acceptance can be extended. In the present E325 setup, the forward acceptance is limited to be larger than 12 degrees, due to the halo intensity. With a small beam-spot size designing the tracking program becomes easier and the momentum resolutions of the charged particle can be significantly improved. The spectrometer should be located in a separated room from the beam dump. Room background is another limitation of the counter operation.

Because the proposed spectrometer has very unique characteristics, the possibilities to deliver slow separated beams like π, K and $\bar{p}$ with a momentum below 2 GeV/c should be considered seriously. The present design of the primary beam line is too long to cope with those particles due to decays.

An idea exists to build another low-momentum beam line on the A line, transfer the beam to the B line and merge with the B line at the very end. By doing so, the B line becomes a very versatile beam channel. We would like to list here the physics possibilities only briefly.

1. slow ϕ meson production with a K^- beam
2. slow ω meson production with a π^- beam
3. exotic search with a $\bar{p}$ beam.

The future plan for light-ion acceleration is very much appreciated in this project. With hadron beams the studies are almost limited within the normal nuclear matter density. Light ions with a 10- to 20-GeV energy are known to be effective to produce high-density nuclear matter. Once knowledge concerning normal nuclear matter has been sufficiently accumulated, studies on higher density matter are a natural way to extend our study in the future.

Spectrometer construction

The experiment is to be performed in two phases. In the first phase, we use the E325 spectrometer with minor modifications. The present limitation of the E325 experiment can be largely overcome once the new beam line has the characteristics described in the previous subsection. The improvements are foreseen in the higher-level trigger logic.

In the second phase, we will re-build the spectrometer while focusing only on electron pair detection with a larger acceptance. To cover a larger acceptance in the target region, one can consider a spectrometer, like HADES at GSI, which utilizes a large toroidal magnet, with RICH

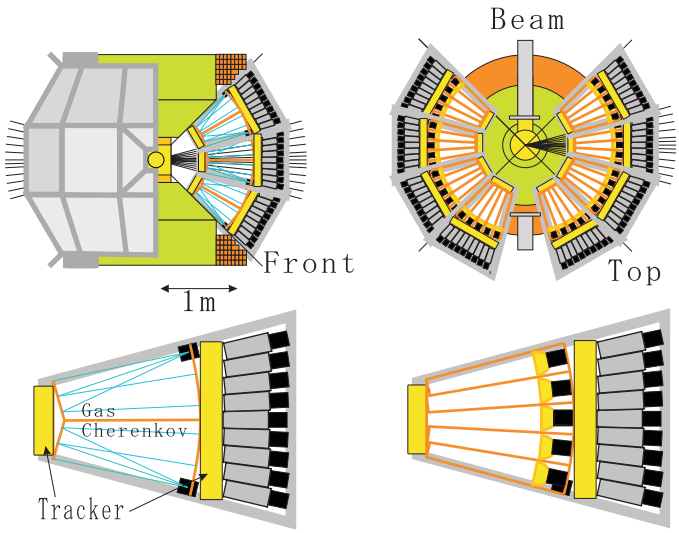

Figure 2.8: Sketch of the new electron spectrometer.

as a major electron-identification device. For the time being, we are considering a completely different approach from HADES, following natural growth from the E325 setup.

A rough sketch is given in Figure 2.8. It is basically a mosaic of 23 identical units, each of which has an aperture of 30 degrees by 30 degrees. The magnet is an axial field type to ensure no practical bending of tracks in the vertical direction. Major electron identification is given by gas Cherenkov counters segmented to 6-degree units vertically and to 15-degree units horizontally. The gas Cherenkov counters are backed up by an electric-magnetic calorimeter segmented to 3 $\times$ 3 degree units. The coincidence width between the front and the back ID counters will be 12 degrees vertically and 15 degrees horizontally

In the E325 spectrometer the segmented units of the gas Cherenkov counters have an aperture of 6 degrees horizontally and 22 degrees vertically. In the trigger level, vertical segmentation was ignored, so that the coincidence window was 24 degrees horizontally and 44 degrees vertically. This segmentation was not perfect to reduce the electron trigger rate. The fine horizontal segmentation was not very useful, due to the bending trajectory, and coarse vertical segmentation was a source of chance coincidence in the trigger level. Those disadvantages in the E325 setup are greatly improved in the new setup.

The resolution of the EM calorimeter will be significantly improved by extending the radiation length by a factor of 3. A well-segmented structure will ensure the measurements of not only electrons, but also photons. One of the interesting measurements becoming available is to detect $K^* \to K^+ + \gamma$ decays, which is another vector meson with a broader width[38].

It turned out in the E325 experiment that the most effective cut for the conversion and the Daliz decays is the opening cut for electron pairs. A trigger will be made by requiring two-fold coincidence of the 30 $\times$ 30 degree units. Tracking devices are located as sandwiching the gas Cherenkov counter. A precise momentum determination can be performed online by assuming a fixed target position, which is determined by the pencil-beam profile and vertical-wire target of about few hundred microns thick.

A phenomenological scaling law is known for the production of narrow vector mesons ($\phi, J/\psi$ or ψ') as

$$\frac{M^3}{\Gamma}\sigma_V(\tau) \propto \frac{1}{\sqrt{\tau}}(1-\sqrt{\tau})^{10}, \tag{2.1}$$

where M is the vector meson mass, Γ is its decay width, $\sigma_V(\tau)$ is the production cross section of a vector meson and $1/\tau = s/M^2$. According to this relation, the ratio of the production cross

sections of ϕ at 12 GeV and 50 GeV is 1:6. The acceptance increase of the spectrometer is about 6. Thus, the expected yield of vector mesons is 100-times (6^3) larger than that of E325, enough to determine the dispersion relation of mesons in nuclear matter.

2.1.3 Summary

The experiment described in this manuscript is to study the fundamental question of quantum chromodynamics, spontaneous breaking of the chiral symmetry, by observing the invariant mass spectrum of hadrons whose properties are subject to be modified due to the partial restoration of chiral symmetry expected in dense nuclear matter.

The experimental feasibility of in-medium meson spectroscopy is demonstrated with the recent results obtained from the KEK-PS E325 experiment, showing hints of nuclear matter modification of vector mesons

We request to develop a new primary beam line which can deliver a pencil beam whose spot size is a few $100\mu m$ with $10^9 \sim 10^{10}$/sec of intensity and with less halo around the beam.

Such a high-quality beam could ensure a robust design of the spectrometer to be built. Preliminary thoughts on the new spectrometer have been given, which should be built in the second phase after re-use of the E325 spectrometer.

2.2 Physics of high-mass dimuon production at the 50-GeV Proton Synchrotron

2.2.1 Introduction

One of the most active areas of research in nuclear and particle physics during the last several decades is the study of quark and gluon distributions in the nucleons and nuclei. Several major surprises were discovered in Deep-Inelastic Scattering (DIS) experiments which profoundly changed our views of the partonic substructure of hadrons. In the early 1980's, the famous 'EMC' effect found in muon DIS provided the first unambiguous evidence that the quark distributions in nuclei are significantly different from those in free nucleons [39, 40]. More recently, surprising results on the spin and flavor structures of the nucleons were discovered in DIS experiments. The so-called 'spin crisis', revealed by the disagreement between the prediction of the Ellis-Jaffe sum rule and the polarized DIS experiments, has led to extensive theoretical and experimental efforts to understand the partonic content of proton's spin [41]. Subsequently, the observation [42] of the violation of the Gottfried sum rule [43] in DIS revealed a surprisingly large asymmetry between the up and down antiquark distributions in the nucleon, shedding new light on the origins of the nucleon sea.

The partonic structure of nucleons and nuclei can also be measured with hadronic probes. A powerful tool for such studies is the Drell-Yan process [44], in which a quark annihilates with an antiquark forming a virtual photon which subsequently decays into a lepton pair. The proton-induced Drell-Yan process is of particular interest, since it can be used to extract antiquark distributions of the target nucleon and nuclei. This provides information complementary to what can be obtained in DIS, which is sensitive to the sum of the quark and antiquark distributions.

The usefulness of the Drell-Yan process as a tool for probing antiquark distributions has been well demonstrated by a series of Fermilab dimuon production experiments [45]. In particular, the Drell-Yan cross section ratios for $p + d$ versus $p + p$ led to a direct measurement of the $\bar{d}/\bar{u}$ asymmetry as a function of Bjorken-x [46, 47]. Furthermore, the nuclear dependence of the Drell-Yan cross sections showed no evidence for antiquark enhancement in heavy nuclei [48], in striking disagreements with predictions of some theoretical models which were capable of explaining the EMC effect.

The 50-GeV Proton Synchrotron (PS) offers a unique opportunity to extend existing measurements of antiquark distributions to much larger values of Bjorken-x. Such information is crucial for understanding the origins of flavor asymmetry in the nucleon sea, and for illuminating the nuclear environment effects on parton distributions. Moreover, Drell-Yan measurements using polarized proton beam on polarized target at the 50-GeV PS will provide a first determination of the spin-dependent antiquark distribution at an x region not accessible in the RHIC-spin program. Indeed, the flavor asymmetry of polarized sea quark distributions, predicted to be very large by certain theoretical models [49, 50], can be directly measured.

A detailed study of the nuclear dependence of Drell-Yan cross sections at 50 GeV could also lead to a first observation of the coherent partonic energy-loss effects predicted recently by Baier, Dokshitser, Mueller, Peigne, Schiff (BDMPS) [51] and by Zakharov [52]. These authors studied the radiative energy loss (through gluon emission) of high energy partons passing through hot and cold hadronic matter. The partonic energy-loss effect is the QCD analog of the Landau-Pomeranchuk-Migdal (LPM) QED effect [53, 54] predicted over 40 years ago and confirmed only recently at SLAC [55]. A number of surprising effects were obtained by BDMPS and Zakharov.

First, the partonic energy loss in a hot QCD plasma is predicted to be much larger than in cold matter. This suggests that an anomalously large energy loss of jets produced in relativistic heavy-ion collisions could be a signature for Quark-Gluon Plasma formation. Second, the radiative energy loss is predicted to be proportional to L^2, where L is the path length of hot or cold nuclear matter traversed by the partons. This curious result is contrary to the conventional wisdom that energy loss depends linearly on L, and it reflects the quantum-mechanical interference effect from several contributing diagrams.

An attempt to search for partonic energy-loss effects in cold matter was made recently via the study of nuclear dependence of Drell-Yan cross sections at 800 GeV [56]. Only an upper limit for partonic energy loss was determined. A much more sensitive study can be made at lower beam energies, where the fractional energy loss $\Delta E/E$ will be larger. At the 50-GeV PS, the effect is expected to be much enhanced and indeed one could even examine whether the nuclear effect follows the L or L^2 dependence.

While logarithmic scaling violation is well established in DIS experiments, no clear evidence for scaling violation has been seen in Drell-Yan process. The 50-GeV PS provides an interesting opportunity for unambiguously establishing scaling violation in the Drell-Yan process [57]. For given values of x_1 and x_2 (Bjorken-x for the projectile and target partons, respectively), scaling-violation is expected to cause roughly a factor of two increase in the Drell-Yan cross sections when proton beam energy is decreased from 800 GeV to 50 GeV. It appears quite feasible to establish scaling violation in the Drell-Yan process with future data from the 50-GeV PS.

Detection of high-mass dileptons at the 50-GeV PS will also allow a study of J/Ψ and Ψ' production. Existing data on proton-induced charmonium production are mostly limited to the energy range 150 GeV $\leq E_p \leq$ 800 GeV. A comparison of 50 GeV charmonium production data with existing data will further improve our knowledge on the production and propagation of charmonium in the nuclear medium. Many different effects which could affect the production of charmonium in nuclear medium, such as nuclear shadowing, partonic energy loss, final-state interaction with comoving gluons or hadrons, will have different beam energy dependences [58, 59]. Therefore, a systematic study of charmonium production in $p-p$, $p-A$ and $A-A$ collisions at 50 GeV would be extremely valuable for disentangling various effects. Only after the mechanisms for charmonium production are well understood could J/Ψ-suppression be used confidently as a signature for Quark-Gluon Plasma formation in relativistic heavy-ion collisions [60, 61].

Many of the proposed studies for Drell-Yan process at the 50-GeV PS could also benefit from the J/Ψ and Ψ' data. Unlike the Drell-Yan which is an electromagnetic process, quarkonium production is a strong-interaction process involving gluon-gluon fusion and quark-antiqaurk fusion. Comparison between the Drell-Yan and quarkonium production data will further elucidate various aspects of parton distributions in nucleons and nuclei, and of the propagation of partons in nuclei. As an example, charmonium production with polarized proton beam at the 50-GeV PS might provide interesting information on the gluon distributions at large Bjorken-x, which is essentially unknown.

In this paper, we discuss the physics interest and the feasibility for making precise measurements of high-mass dimuons at the 50-GeV PS. In Section 2.2.2 the physics motivation for various measurements will be discussed in some details. A preliminary design study of a dimuon spectrometer for the 50-GeV PS will be presented in Section 2.2.3. A summary is given in Section 2.2.4.

2.2.2 Physics Issues

Overview of high-mass dilepton production

Detection of high-mass dileptons produced in high-energy hadronic interactions has a long and glorious history. The charm and beauty quarks were discovered in the 1970's via the dilepton decay modes of J/Ψ and Υ resonances. These quarkonium states are superimposed on a dilepton continuum known as the Drell-Yan process [44]. The Drell-Yan data has been a source of information for the antiquark structure of the nucleon [62]. Furthermore, Drell-Yan production with pion and kaon beams has yielded the parton distributions of these unstable particles for the first time. A generalized Drell-Yan process was also responsible for the discovery of the W and Z gauge bosons in the 1980's.

To lowest order, the Drell-Yan process depends on the product of quark and antiquark distributions in the beam and target as

$$\frac{d^2\sigma}{dx_1 dx_2} = \frac{4\pi\alpha^2}{9s\ x_1 x_2} \sum_a e_a^2 [q_a(x_1)\bar{q}_a(x_2) + \bar{q}_a(x_1) q_a(x_2)]. \tag{2.2}$$

Here $q_a(x)$ are the quark or antiquark structure functions of the two colliding hadrons evaluated at momentum fractions x_1 and x_2. The sum is over quark flavors, and s is the center-of-mass energy squared.

The kinematics of the virtual photon – longitudinal center-of-mass momentum $p_{||}^{\gamma}$, transverse momentum p_T^{γ} and mass M_{γ} – are determined by measuring the two-muon decay of the virtual photon. These quantities determine the momentum fractions of the two quarks:

$$x_F = p_{||}^{\gamma}/p_{||}^{\gamma,max} = x_1 - x_2 \tag{2.3}$$

$$M_{\gamma}^2 = x_1 x_2 s \tag{2.4}$$

where $p_{||}^{\gamma}$ is the virtual photon center-of-mass longitudinal momentum and $p_{||}^{\gamma,max}$ is the maximum value it can have.

Although the simple parton model enjoyed considerable success in explaining many features of the early data, it was soon realized that QCD corrections to the parton model were required. The inclusion of the NLO diagrams for the Drell-Yan process brings excellent agreement between the calculations and the data. As an example, Figure 2.9 shows the NA3 data [63] at 400 GeV, together with the E605 [64] and E772 [65] data at 800 GeV. The solid curves in Figure 2.9 correspond to NLO calculation for 800 GeV $p + d$ ($\sqrt{s}$ = 38.9 GeV) and they describe the NA3/E605/E772 data well. This shows that the mechanism for Drell-Yan process is well understood theoretically, and quantitative information on the parton distributions can be reliably extracted via this process.

To gain sensitivity to the antiquark distribution of the target, one chooses a proton beam and selects the kinematic region of positive x_F and large x_1. In this limit the contribution from the second term in Eq. 2.2 is small and the first term is dominated by the $u(x_1)$ distribution of the proton. Under these circumstances, the ratio of the cross sections for two different targets, X and Y, which have A_X and A_Y nucleons is approximately the ratio of the $\bar{u}(x_2)$ distributions:

$$\frac{\frac{1}{A_X}\left(\frac{d\sigma^X}{dx_1 dx_2}\right)}{\frac{1}{A_Y}\left(\frac{d\sigma^Y}{dx_1 dx_2}\right)} \approx \left.\frac{\bar{u}^X(x_2)}{\bar{u}^Y(x_2)}\right|_{x_1 \gg x_2} \tag{2.5}$$

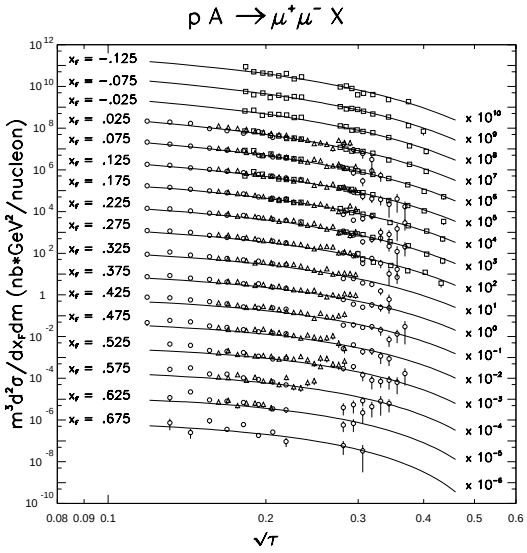

Figure 2.9: Proton-induced Drell-Yan production from experiments NA3 [63] (triangles) at 400 GeV/c, E605 [64] (squares) at 800 GeV/c, and E772 [65] (circles) at 800 GeV/c. The lines are absolute (no arbitrary normalization factor) next-to-leading order calculations for $p+d$ collisions at 800 GeV/c using the CTEQ4M structure functions [66].

In this relation the cross sections are defined per nucleus but the parton distributions are conventionally defined per nucleon.

Eq. 2.5 demonstrates the power of Drell-Yan experiments in determining relative antiquark distributions. This feature was explored by recent Fermilab experiments using 800 GeV proton beams [45]. The 50-GeV PS provides a unique opportunity for extending the Fermilab measurements to larger x_2 ($x_2 > 0.25$). For a given value of x_1 and x_2, the Drell-Yan cross section is proportional to $1/s$ (see Eq. 2.2). Hence the cross section at 50 GeV is roughly 16 times greater than that at 800 GeV (The price one pays at lower beam energies is that one has limited reach for small x_2, which could best be studied at higher energies). Furthermore, to the extent that the radiation dose scales as beam power, one can take $\approx$ 16 times higher beam flux at 50 GeV relative to 800 GeV. The combination of these two effects could lead to two orders of magnitude improvement in the statistics at high x_2 over previous Fermilab experiments.

Scaling violation in Drell-Yan process

The right-hand side of Eq. 2.2 is only a function of x_1, x_2 and is independent of the beam energy. This scaling property no longer holds when QCD corrections to the Drell-Yan process are taken into account. While scaling violation is well established in DIS experiments, it is not confirmed in Drell-Yan experiments at all. No convincing evidence for scaling violation is seen [67]. As discussed in a recent review [45], there are mainly two reasons for this. First, unlike the DIS, the Drell-Yan cross section is a convolution of two structure functions. For proton-induced Drell-Yan, one often involves a beam quark with $x_1 > 0.1$ and a target antiquark with $x_2 < 0.1$. Scaling violation implies that the structure functions rise for $x \leq 0.1$ and drop for $x \geq 0.1$ as Q^2 increases. Hence the effects of scaling violation are partially cancelled. Second, unlike the

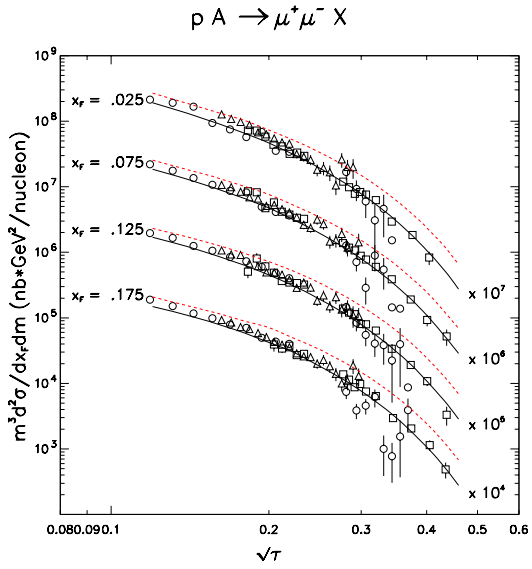

Figure 2.10: Comparison of Drell-Yan cross section data with NLO calculations using MRST [68] structure functions. Note that $\tau = x_1 x_2$. The E772 [65], E605 [64], and NA3 [63] data points are shown as circles, squares, and triangles, respectively. The solid curves correspond to fixed-target $p + d$ collision at 800 GeV, while the dashed curve is for $p + d$ collision at 50 GeV.

DIS, the Drell-Yan experiment can only probe relatively large Q^2, namely, $Q^2 > 16$ GeV^2 for a mass cut of 4 GeV. This makes it more difficult to observe the logarithmic Q^2 variation of the structure functions in Drell-Yan experiments.

The 50-GeV PS provides an interesting opportunity for unambiguously establishing scaling violation in the Drell-Yan process. Figure 2.10 shows the predictions for $p+d$ at 50 GeV. Scaling violation causes a factor of two increase in the Drell-Yan cross sections when the beam energy is decreased from 800 GeV to 50 GeV. It appears quite feasible to establish scaling violation in Drell-Yan with future dilepton production experiments at the 50-GeV PS.

$\bar{d}/\bar{u}$ asymmetry of the proton

From neutrino-induced DIS experiments, it is known that the strange quark sea in the nucleon is roughly a factor of two less than the up or down quark sea [69]. The lack of SU(3) flavor symmetry in the nucleon sea is attributed to the much heavier mass of the strange quark. Until recently, it had been assumed that the distributions of $\bar{u}$ and $\bar{d}$ quarks were identical. Although the equality of $\bar{u}$ and $\bar{d}$ in the proton is not required by any known symmetry, this is a plausible assumption for sea quarks generated by gluon splitting. Because the masses of the up and down quarks are small compared to the confinement scale, nearly equal numbers of up and down sea quarks should result.

The assumption of $\bar{u}(x) = \bar{d}(x)$ can be tested by measurements of the Gottfried integral [43], defined as

$$I_G = \int_0^1 \left[F_2^p(x,Q^2) - F_2^n(x,Q^2)\right]/x \; dx = \frac{1}{3} + \frac{2}{3}\int_0^1 \left[\bar{u}_p(x) - \bar{d}_p(x)\right] dx, \qquad (2.6)$$

where F_2^p and F_2^n are the proton and neutron structure functions measured in DIS experiments.

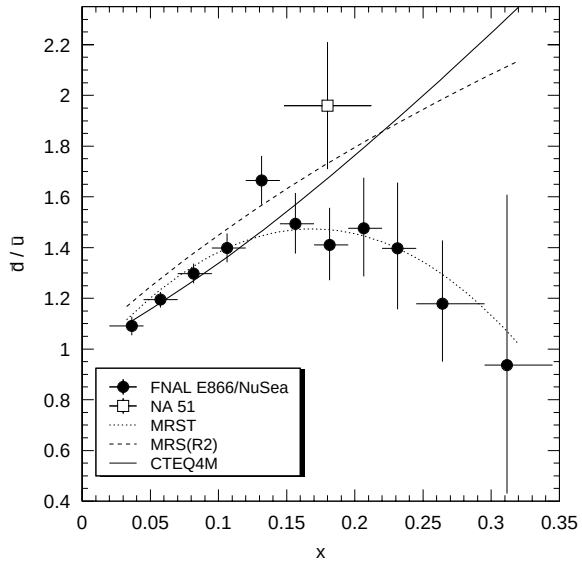

Figure 2.11: The ratio of $\bar{d}/\bar{u}$ in the proton as a function of x extracted from the Fermilab E866 [46] cross section ratio. The curves are from various parton distributions. Also shown is the result from NA51 [72], plotted as an open square.

Under the assumption of a symmetric sea, $\bar{u} = \bar{d}$, the Gottfried Sum Rule (GSR) [43], $I_G = 1/3$, is obtained. The most accurate test of the GSR was reported in 1991 by the New Muon Collaboration (NMC) [42], which measured F_2^p and F_2^n over the region $0.004 \leq x \leq 0.8$. They determined the Gottfried integral to be 0.235 ± 0.026, significantly below 1/3. This surprising result has generated much interest, and it strongly suggested that the assumption $\bar{u} = \bar{d}$ should be abandoned. Specifically, the NMC result implies

$$\int_0^1 [\bar{d}(x) - \bar{u}(x)]\, dx = 0.148 \pm 0.039. \tag{2.7}$$

Eq. 2.7 shows that only the integral of $\bar{d} - \bar{u}$ was deduced from the DIS measurements. The x dependence of $\bar{d} - \bar{u}$ remained unspecified.

The proton-induced Drell-Yan process provides an independent means to probe the flavor asymmetry of the nucleon sea [70]. An important advantage of the Drell-Yan process is that the x dependence of $\bar{d}/\bar{u}$ can be determined. The Fermilab E772 collaboration [71] compared the Drell-Yan yields from isoscalar targets with that from a neutron-rich (tungsten) target, and constraints on the nonequality of $\bar{u}$ and $\bar{d}$ in the range $0.04 \leq x \leq 0.27$ were set. More recently, the CERN experiment NA51 [72] carried out a comparison of the Drell-Yan muon pair yield from hydrogen and deuterium using a 450 GeV/c proton beam. They found that $\bar{u}/\bar{d} = 0.51 \pm 0.04 \pm 0.05$ at $\langle x \rangle = 0.18$, a surprisingly large difference between the $\bar{u}$ and $\bar{d}$.

A Drell-Yan experiment (E866), aiming at higher statistical accuracy and wider kinematic coverage than NA51, was recently completed [46, 47] at Fermilab. This experiment also measured the Drell-Yan muon pairs from 800-GeV/c protons interacting with liquid deuterium and hydrogen targets. Eq. 2.5 shows that the Drell-Yan cross section ratio at large x_F is approxi-

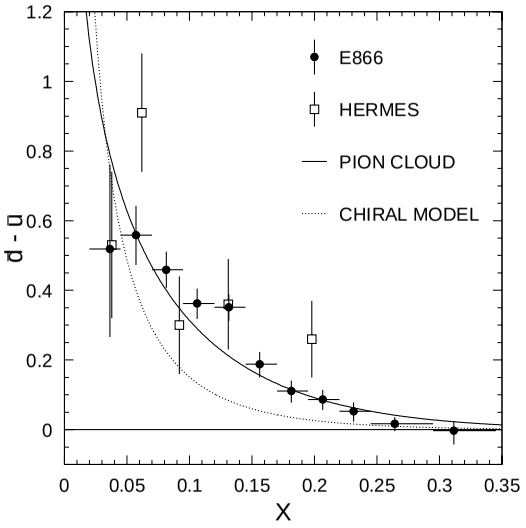

Figure 2.12: Comparison of the E866 [46] $\bar{d}-\bar{u}$ results at $Q^2 = 54$ GeV^2/c^2 with the predictions of pion-cloud and chiral models as described in the text. The data from HERMES [80] are also shown.

mately given as

$$\frac{\sigma_{DY}(p+d)}{2\sigma_{DY}(p+p)} \approx \frac{1}{2}\left(1+\frac{\bar{d}(x_2)}{\bar{u}(x_2)}\right). \tag{2.8}$$

Values for $\bar{d}/\bar{u}$ were extracted by the E866 collaboration at $Q^2 = 54$ GeV^2/c^2 over the region $0.02 < x < 0.345$. These are shown in Figure 2.11 along with the NA51 measurement. For $x < 0.15$, $\bar{d}/\bar{u}$ increases linearly with x and is in good agreement with the CTEQ4M [66] and MRS(R2) [73] parameterizations. However, a distinct feature of the data, not seen in either parameterization, is the rapid decrease toward unity of $\bar{d}/\bar{u}$ beyond $x = 0.2$.

The $\bar{d}/\bar{u}$ ratio, along with the CTEQ4M values for $\bar{d}+\bar{u}$, was used to obtain $\bar{d}-\bar{u}$ (Figure 2.12). Being a flavor nonsinglet quantity, $\bar{d}(x) - \bar{u}(x)$ is decoupled from gluon distribution. Since perturbative processes have negligible contribution to $\bar{d}/\bar{u}$ asymmetry, $\bar{d}(x) - \bar{u}(x)$ essentially isolates the contribution from non-perturbative effects. From the results shown in Figure 2.12, one can obtain an independent determination [47] of the integral of Eq. 2.7. E866 finds $0.100 \pm 0.007 \pm 0.017$, consistent with, but roughly 2/3 of the value deduced by NMC.

As early as 1983, Thomas [74] pointed out that the virtual pions that dress the proton will lead to an enhancement of $\bar{d}$ relative to $\bar{u}$ via the (nonperturbative) "Sullivan process." Sullivan [75] previously showed that in DIS virtual mesons scale in the Bjorken limit and contribute to the nucleon structure function. Following the publication of the NMC result, many papers treated virtual mesons as the origin of the $\bar{d}/\bar{u}$ asymmetry (see [76] for a recent review). Here the $\pi^+(\bar{d}u)$ cloud, dominant in the process $p \to \pi^+ n$, leads to an excess of $\bar{d}$ sea.

A different approach for including the effects of virtual mesons has been presented by Eichten et al. [77] and further investigated by other authors [78, 79]. In chiral perturbation theory, the relevant degrees of freedom are constituent quarks, gluons, and Goldstone bosons. In this model, a portion of the sea comes from the couplings of Goldstone bosons to the constituent quarks, such as $u \to d\pi^+$ and $d \to u\pi^-$. The excess of $\bar{d}$ over $\bar{u}$ is then simply due to the additional valence u quark in the proton.

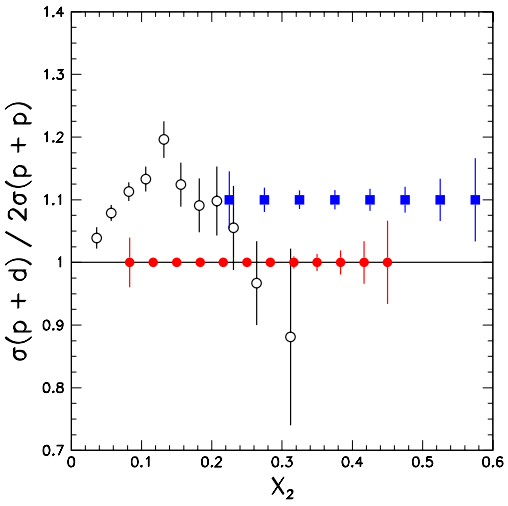

Figure 2.13: $(p+d)/(p+p)$ Drell-Yan ratios from E866 (open circles) are compared with the expected sensitivites at the 120 GeV Main Injector (solid circles) and the 50-GeV PS (solid squares).

The x dependence of $\bar{d}-\bar{u}$ and $\bar{d}/\bar{u}$ obtained by E866 provides important constraints for theoretical models. Figure 2.12 compares $\bar{d}(x)-\bar{u}(x)$ from E866 with a virtual-pion model calculation, following the procedure detailed by Kumano [81]. A dipole form, with $\Lambda = 1.0$ GeV for the πNN form factor and $\Lambda = 0.8$ GeV for the $\pi N\Delta$ form factor, was used. Λ is the cutoff parameter for the pion form factor. Figure 2.12 also shows the predicted $\bar{d}-\bar{u}$ from the chiral model [79]. The chiral model places more strength at low x than does the virtual-pion model. This difference reflects the fact that the pions are softer in the chiral model, since they are coupled to constituent quarks that carry only a fraction of the nucleon momentum. The x dependence of the E866 data favors the virtual-pion model over the chiral model, suggesting that correlations between the chiral constituents should be taken into account.

Recently, the flavor asymmetry of the nucelon sea was computed in the large-N_c limit, where the nucleon is described as a soliton of an effective chiral theory [50, 82]. In this chiral quark-soliton model, the flavor non-singlet distribution, $\bar{d}(x)-\bar{u}(x)$, appears in the next-to-leading order of the $1/N_c$ expansion [49]. The E866 $\bar{d}(x)-\bar{u}(x)$ data were shown to be well described by this model [82].

Instantons have been known as theoretical constructs since the seventies [83, 84, 85]. They represent non-perturbative fluctuations of the gauge fields that induce transitions between degenerate ground states of different topology. In the case of QCD, the collision between a quark and an instanton flips the helicity of the quark while creating a $q\bar{q}$ pair of different flavor. Thus, interaction between a u quark and an instanton results in a u quark of opposite helicity and either a $d\bar{d}$ or $s\bar{s}$ pair. Such a model has the possibility of accounting for both the flavor asymmetry and the "spin crisis" [86, 87]. However, the prediction [88] at large x, $\bar{d}(x)/\bar{u}(x) \to 4$, is grossly violated by experiment (see Figure 2.11). Thus, it appears that while instantons have the possibility for accounting for flavor and spin anomalies, the approach is not yet sufficiently developed for a direct comparison.

The interplay between the perturbative and non-perturbative components of the nucleon sea remains to be better determined. Since the perturbative process gives a symmetric $\bar{d}/\bar{u}$ while a

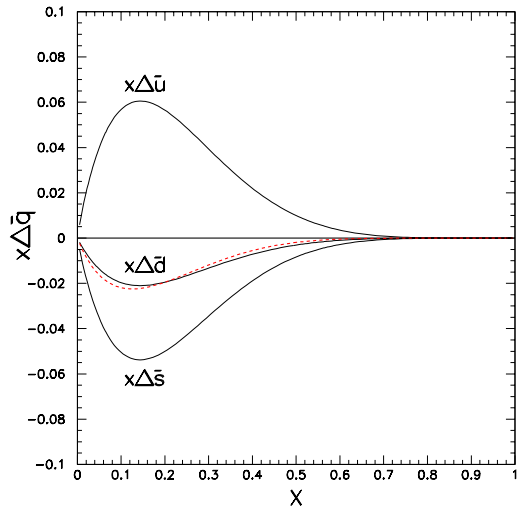

Figure 2.14: Sea quark polarizations at Q^2=0.36 GeV^2 predicted by chiral-quark soliton model are shown as solid curves. The dashed curve corresponds to the parametrization of $x\Delta\bar{q}$ at $Q^2 = 0.4\text{GeV}^2$ by GRSV, where $\Delta\bar{q} = \Delta\bar{u} = \Delta\bar{d} = \Delta\bar{s}$.

non-perturbative process is needed to generate an asymmetric $\bar{d}/\bar{u}$ sea, the relative importance of these two components is directly reflected in the $\bar{d}/\bar{u}$ ratios. Thus, it would be very important to extend the Drell-Yan measurements to kinematic regimes beyond the current limits.

The 50-GeV PS presents an excellent opportunity for extending the $\bar{d}/\bar{u}$ measurement to larger x ($x > 0.25$). As mentioned earlier, for given values of x_1 and x_2 the Drell-Yan cross section is proportional to $1/s$, hence the Drell-Yan cross section at 50 GeV is roughly 16 times greater than at 800 GeV. Figure 2.13 shows the expected statistical accuracy for $\sigma(p+d)/2\sigma(p+p)$ at the 50-GeV PS (see Section 2.2.3) compared with the data from E866 and a proposed measurement [89] using the 120 GeV proton beam at the Fermilab Main-Injector. A definitive measurement of the $\bar{d}/\bar{u}$ over the region $0.25 < x < 0.7$ could indeed be obtained at the 50-GeV PS.

Polarized Drell-Yan at the 50-GeV PS

Despite extensive work on polarized DIS, the helicity distributions of $\bar{u}$ and $\bar{d}$ sea quarks are still poorly known. Both the SMC [90] and the HERMES [91] experiments attempted to extract the sea-quark polarizations via semi-inclusive polarized DIS measurements, and the results indicate small sea-quark polarization consistent with zero. However, as pointed out in Ref. [92], large uncertainties are associated with certain assumptions made in the extraction.

A direct measurement of sea-quark's polarization is clearly very important for understanding the flavor decomposition of proton's spin. Different theoretical models make drastically different predictions. In particular, the meson-cloud models, which successfully describe the unpolarized $\bar{d}/\bar{u}$ asymmetry, predict negligible amount of sea-quark polarization [93, 94]. Several current parametrizations [95, 96] of polarized parton distributions also assume very small polarization for sea quarks. The chiral-quark soliton model, on the other hand, predicts substantial sea-quark polarization [49, 92]. Figure 2.14 shows $x\Delta\bar{u}(x)$, $x\Delta\bar{d}(x)$, and $x\Delta\bar{s}(x)$ at $Q_0^2 = 0.36$ GeV^2 from a recent prediction of chiral-quark soliton model [97]. Also shown in Figure 2.14 are the GRSV

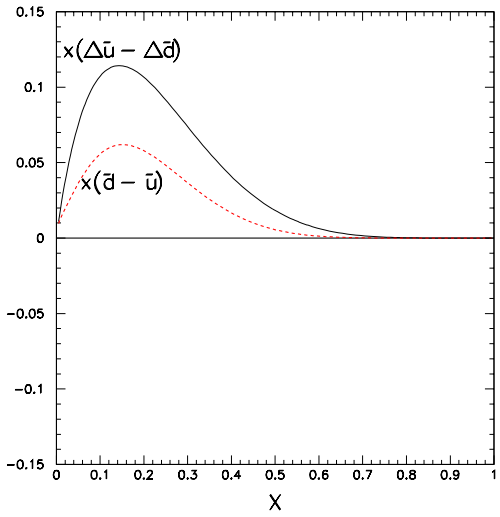

Figure 2.15: $x(\Delta\bar{u} - \Delta\bar{d})$ at $Q^2 = 0.36$ GeV^2 predicted by the chiral-quark soliton model is shown as the solid curve. The GRV94 LO parametrization of $x(\bar{d} - \bar{u})$ at $Q^2 = 0.4$ GeV^2 is shown as the dashed curve.

parametrizations [96] from a global fit to polarized DIS data.

A very striking prediction of the chiral-quark model is the large flavor asymmetry of polarized sea-quark polarization. In fact, this model predicts a significantly larger values for $\Delta\bar{u} - \Delta\bar{d}$ than for $\bar{d} - \bar{u}$. This is shown in Figure 2.15, where $x(\Delta\bar{u} - \Delta\bar{d})$ from the chiral-quark soliton model [97] is compared with the $x(\bar{d} - \bar{u})$ parametrization from GRV94 [98].

Polarized proton beam at the 50-GeV PS would offer an exciting opportunity for probing sea-quark polarizations. The longitudinal spin asymmetry in the DY process is, in leading order, given by [99],

$$A_{LL}^{DY}(x_1, x_2) = \frac{\sum_a e_a^2[\Delta q_a(x_1)\Delta\bar{q}_a(x_2) + \Delta\bar{q}_a(x_1)\Delta q_a(x_2)]}{\sum_a e_a^2[q_a(x_1)\bar{q}_a(x_2) + \bar{q}_a(x_1)q_a(x_2)]}, \tag{2.9}$$

with $\Delta q_a \equiv q_a^+ - q_a^-$. The superscripts refer to parton spin projections parallel $(+)$ or antiparallel $(-)$ to the proton's spin projection. We have simulated the performance of the proposed high-mass dimuon spectrometer for measuring polarized antiquark distribution. Figure 2.16 shows the x_2 dependence of A_{LL}^{DY}, integrated over the spectrometer acceptance, for polarized sea-quark parametrizations including Gehrmann-Stirling (G-S) sets A and C [95] and GRSV Leading-Order set [96]. Very small values for A_{LL}^{DY} are predicted for the G-S parametrization, while the GRSV parametrization gives $A_{LL}^{DY} \approx -0.2$. The chiral-quark soliton model gives large positive A_{LL}^{DY}. In fact, the positivity requirement, namely, $-1 < \Delta\bar{u}(x)/\bar{u}(x) < 1$, is not always satisfied at the region $x > 0.2$ for the particular parametrization given by Ref. [97].

We have calculated the expected statistical sensitivities for a 120-day $\vec{p} + \vec{p}$ measurement, assuming 75% polarization for a 5×10^{11} per spill polarized proton beam. We also assume a polarized solid NH_3 target similar to the one used by the SMC [100] which achieves a hydrogen polarization of 75% and a dilution factor of 0.15. The target length is chosen to give the same gm/cm^2 as for the liquid deuterium target. Figure 2.16 shows that the statistical accuracy of such a measurement can well test the predictions of various model (note that the chiral-quark soliton model predicts a large positive A_{LL}^{DY} not shown in this figure). A comparison of $\vec{p} + \vec{p}$

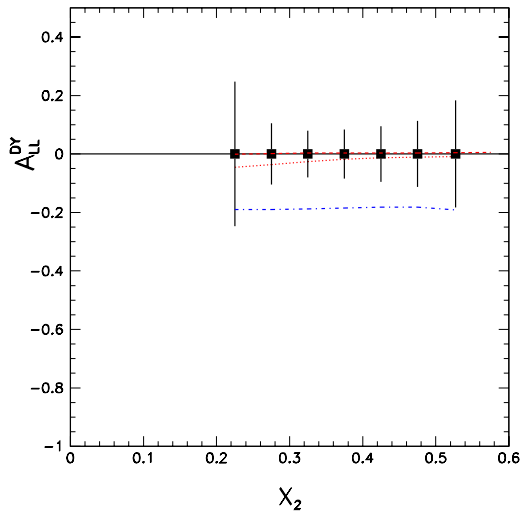

Figure 2.16: Expected statistical accuracy for measuring the double-helicity asymmetry A_{LL}^{DY} in polarized $p + p$ Drell-Yan at the 50-GeV PS for a 120-day run. The dashed, dotted, and dash-dotted curves correspond to calculations using polarized PDF parametrization of G-S (set A, set C) and GRSV, respectively.

with $\vec{p} + \vec{d}$ will further determine $\Delta\bar{d}$, which provides a direct test of the chiral-quark soliton model's prediction of large $\Delta\bar{u} - \Delta\bar{d}$.

In the polarized Drell-Yan process one may also measure a new structure function, called transversity, which is a correlation between quark momentum and its perpendicular spin component [101]. The transversity is not measurable in inclusive DIS [102]. It is measurable, in principle, in collisions of polarized protons whose spins are aligned perpendicular to the plane of dilepton detection [103]. A non-zero transverse spin correlation in the Drell-Yan process would clearly require both quark and antiquark transversities to be non-zero. Polarized proton beam at the 50-GeV PS could provide unique information on the transversities at large x.

Nuclear effects of Drell-Yan

Following the discovery of the EMC effect, it was suggested [104, 105, 106] that this effect is caused by the excess of virtual pions in nuclei, which significantly modify the nuclear parton distributions. A direct consequence of the "pion-excess" model is the nuclear enhancement of antiquark sea, which can be probed via Drell-Yan experiment [107]. However, the subsequent Fermilab E772 experiment [48] found no evidence for such enhancement (see Figure 2.17). The lack of an antiquark enhancement in nuclei suggests that there are no more pions surrounding an average nucleon in a heavy nucleus than there are in a weakly bound system, deuterium. This contradicts conventional wisdom and is also at odds with sophisticated calculations using realistic nuclear force [108]. Unfortunately, the error bars for the E772 data in the region $x > 0.15$ become quite large, due entirely to limited statistics. Furthermore, at $x < 0.1$ the on-set of the shadowing effect makes the isolation of possible pion-excess effect somewhat uncertain.

At the 50-GeV PS, one can measure the nuclear effect over the large x region ($x > 0.15$) with high accuracy. This is illustrated in Figure 2.17, where the expected statistical errors for a 60-day measurement of $p + Ca$ and $p + d$ using the proposed spectrometer (see Section 2.2.3)

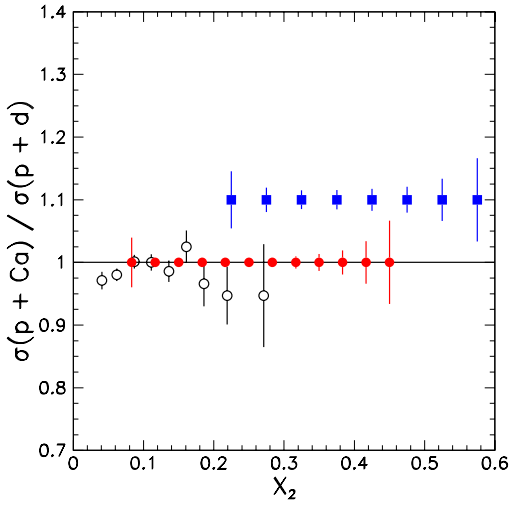

Figure 2.17: $(p + Ca)/(p + d)$ Drell-Yan ratios from E772 (open circles) are compared with the expected sensitivites at the 120 GeV Main Injector (solid circles) and at the 50 GeV PS (solid squares).

are shown. One advantage of the 50-GeV measurement is that shadowing effect is no longer important at large x. The precise measurement at x larger than E772 could access would provide extremely valuable new information on the nuclear dependence of antiquark distributions. The anticipated sensitivity will be sufficient to observe the reduction in the nuclear sea distributions predicted in the Q^2 rescaling models [109]. The pion-excess model, on the other hand, predicts a strong nuclear enhancement of Drell-Yan cross sections in this x region.

Partonic energy loss in nuclei

The subject of energy loss of fast partons propagating through hadronic matters has attracted considerable interest recently [110]. The nuclear dependence of the Drell-Yan process provides a particularly clean way to measure the energy loss of incident quarks in a cold nuclear medium. Partonic energy loss would lead to a degradation of the quark momentum prior to annihilation, resulting in a less energetic muon pair. Therefore, one expects the Drell-Yan cross sections for heavier nuclear targets to drop more rapidly at large x_1 (or x_F).

Data from E772 at 800 GeV/c were analysed by Gavin and Milana [111] to deduce the initial-state quark energy loss. They ignored the shadowing effect and assumed the following expression for the average change in the momentum fraction:

$$\Delta x_1 = -\kappa_1 x_1 A^{1/3}. \tag{2.10}$$

A surprisingly large fractional energy loss ($\approx 0.4\%/fm$) was obtained. This result was questioned by Brodsky and Hoyer [112], who argued that the time scale for gluon bremsstrahlung need to be taken into account. Moreover, as pointed out in Ref. [45], it is important to account for the shadowing effect before a reliable value of partonic energy loss can be extracted. Using an analogy to the photon bremsstrahlung process, Brodsky and Hoyer suggested an alternative expression:

$$\Delta x_1 \approx -\frac{\kappa_2}{s} A^{1/3}, \tag{2.11}$$

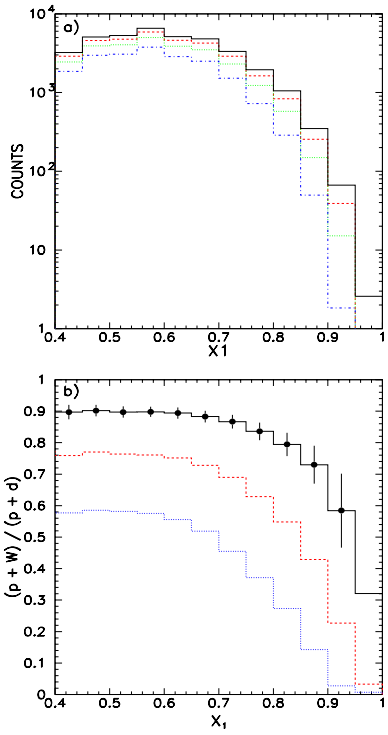

Figure 2.18: a): Solid curve is the expected $p + d$ spectrum for a 60-day run at 50 GeV. The dashed, dotted, and dash-dotted curves correspond to $p+W$ spectra assuming a partonic energy loss rate of 0.1, 0.25, 0.5 GeV/fm, respectively. b): Solid circles show the expected statistical errors for $(p+W)/(p+d)$ ratios in a 60-day run for $p+W$ and $p+p$ each. The solid, dashed, and dotted curves correspond to a partonic energy loss rate of 0.1, 0.25, 0.5 GeV/fm, respectively.

where s is the square of the nucleon-nucleon center-of-mass energy. Note that Eq. 2.10 implies a linear dependence of the energy loss on the partonic energy, while Eq. 2.11 assumes a constant energy loss independent of the partonic energy (note that ΔE is proportional to $\Delta x_1 s$). Based on uncertainty principle, Brodsky and Hoyer concluded that energetic partons should loose ≤ 0.5 GeV/fm in nuclei. More recently, Baier et al. [51] and Zakharov [52] predicted

$$\Delta x_1 \approx -\frac{\kappa_3}{s} A^{2/3}. \tag{2.12}$$

These authors obtained the nonintuitive result that the total energy loss is proportional to the square of the path length traversed.

Very recently, the E866 nuclear-dependence data have been analysed by taking into consideration the shadowing effect and comparing with the three different expressions (Eqs. 2.10 - 2.12) for energy loss [56]. Upper limits of $\kappa_2 < 0.75$ GeV^2 and $\kappa_3 < 0.10$ GeV^2 have been obtained. The κ_2 limit corresponds to a constant energy loss rate of < 0.44 GeV/fm, while the κ_3 limit implies $\Delta E < 0.046$ GeV/fm$^2 \times L^2$, where L is the quark propagation length through the nucleus. This is very close to the lower value given by Baier et al. [51] for cold nuclear matter.

A much more sensitive study of the partonic energy loss could be carried out at the 50-GeV PS. We have simulated the effect of initial-state energy loss on the $p + W$ Drell-Yan cross sections, and the results are shown in Figure 2.18. Assuming a 60-day run with the nominal spectrometer configuration (see Section 2.2.3), the expected x_1 distribution for $p + d$ is shown

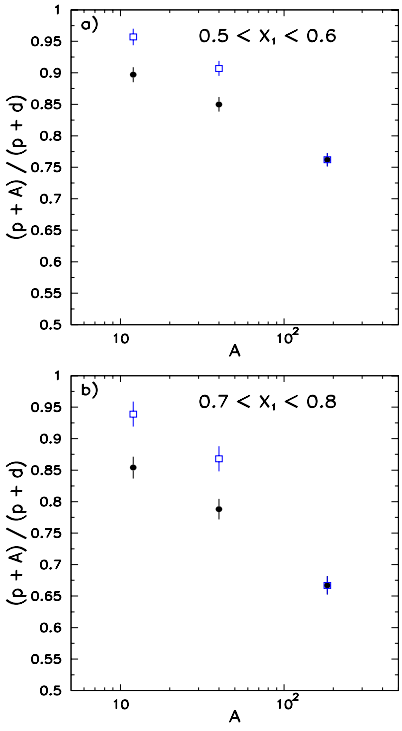

Figure 2.19: a): Solid circles correspond to the expected $(p + A)/(p + d)$ ratios assuming a partonic energy loss rate of 0.25 GeV/fm with a nuclear dependence given by Eq. 2.11. The open squares correspond to partonic energy loss given by Eq. 2.12. The statistical erorrs were calculated assuming a 60-day run for each target. b) Same as the top figure, but for a different x_1 bin $(0.7 < x < 0.8)$.

as the solid curve. The dashed, dotted, and dash-dotted curves in Figure 2.18 correspond to $p+W$ x_1 spectra assuming a partonic energy loss form of Eq. 2.11 with dE/dz of -0.1, -0.25, -0.5 GeV/fm, respectively. The ratios of $p + W$ over $p + d$, shown in Figure 2.18, are very sensitive to the quark energy loss rate, and the expected statistical accuracy can easily identify an energy loss as small as 0.1 GeV/fm. The greater sensitivity at 50 GeV is due to the $1/s$ factor in Eq. 2.11 and Eq. 2.12. Another important advantage at 50 GeV is the absence of shadowing effect, and no shadowing correction is required.

The Drell-Yan A-dependence data could further be used to determine whether the energy loss follows an L (as in Eq. 2.11) or an L^2 (as in Eq. 2.12) dependence. This is illustrated in Figure 2.19, where the solid circles correspond to $(p + A)/(p + d)$ assuming an energy-loss rate of 0.25 GeV/fm using Eq. 2.11. The open squares correspond to the situation when energy loss is described by Eq. 2.12 (the value of κ_3 is selected by matching the $(p + W)/(p + d)$ values for both cases). Figure 2.19 shows that one can easily distinguish an L- from an L^2-dependence even when the energy loss rate is as small as 0.25 GeV/fm.

Quarkonium Production at 50 GeV

Unlike the Drell-Yan process, the mechanisms for J/Ψ production are not well understood. Several quarkonium production models have been considered in the literature, including color-evaporation, color-singlet, and color-octet models. For simplicity, we consider the color-

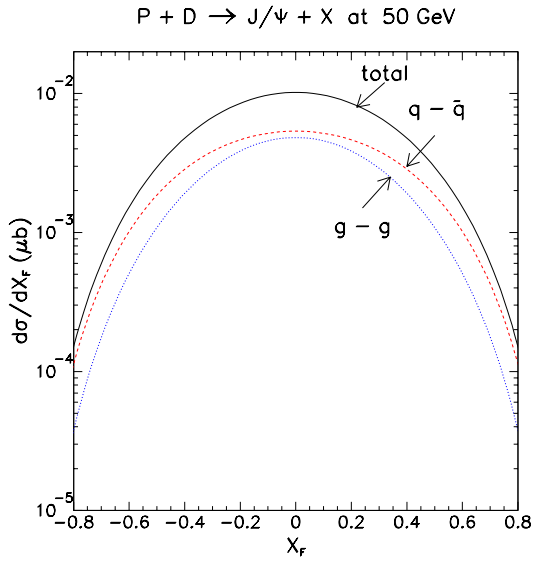

Figure 2.20: Calculation of the $p + d \rightarrow J/\Psi + x$ cross sections at 50 GeV using the color-evaporation model. The contributions from the gluon-gluon fusion and the quark-antiquark annihilation subprocesses are also shown.

evaporation model, which is capable of describing the energy-dependence and the shape of the differential cross sections well. However, the absolute normalization of this model is treated as a parameter.

Figure 2.20 shows the prediction of the color-evaporation model for J/Ψ production at 50 GeV. The absolute normalization is obtained from an extrapolation of the global fit of existing J/Ψ data [113]. Unlike the situation at 800 GeV where the gluon-gluon fusion subprocess dominates [114], Figure 2.20 shows that the quark-antiquark annihilation is the dominant subprocess at 50 GeV. While this is reminescent of the Drell-Yan process, it is worth noting that quarkonium production is a hadronic process unlike the electromagnetic Drell-Yan process. Hence, there is no e_q^2 weighting factor for the $q - \bar{q}$ subprocess in J/Ψ production.

As indicated in Figure 2.20, the J/Ψ production data at 50 GeV are largely sensitive to quark distributions and could provide information similar to Drell-Yan. This is illustrated in Figure 2.21 which shows that the J/Ψ cross section ratio for $p+d$ over $p+p$ is very sensitive to the $\bar{d}/\bar{u}$ asymmetry just like the Drell-Yan process. This could be readily tested at the 50-GeV PS, since the J/Ψ event rate is expected to be very high.

It is also of interest to measure J/Ψ production using polarized proton beam and target. Unfortunately, the uncertainty of the production mechanism might make it difficult to deduce information on polarized structure functions.

2.2.3 Experimental Apparatus

The spectrometer considered here is designed to measure muon pairs at $M_{\mu^+\mu^-} \geq 1$ GeV with 50 GeV proton beam. The E866 spectrometer and its daughter, a proposed P906 spectrometer [89], are taken as a starting point. The E866 spectrometer is shown in Figure 2.22. $\mu^+\mu^-$ pairs produced at the target were analyzed by a vertical-bending spectrometer. The remaining proton beam was intercepted by a copper beam dump located inside the dipole magnet. The beam dump was followed by a set of absorbers made of copper, carbon, and polyethylene, which

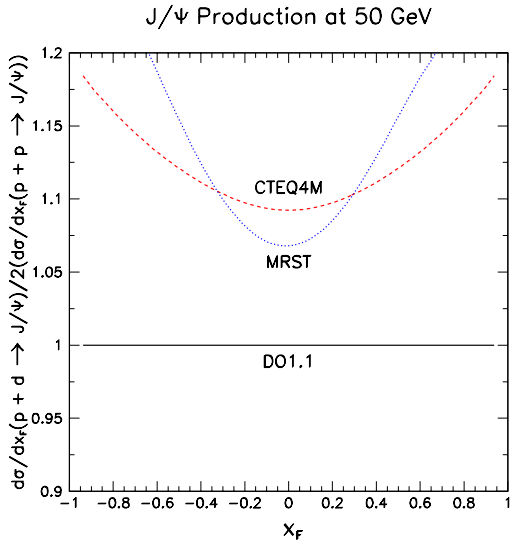

Figure 2.21: Calculations of the $p + d \rightarrow J/\Psi$ over $p + p \rightarrow J/\Psi$ ratios at 50 GeV using the color-evaporation model. The $\bar{d}/\bar{u}$-symmetric structure functions DO1.1 and the $\bar{d}/\bar{u}$ asymmetric structure functions (MRST and CTEQ4M) have been used in these calculations.

absorbed many of the pions and kaons produced at the target before they could decay into muon backgrounds. Trigger hodoscopes, muon identifiers, and tracking counters followed the magnets. The magnetic current can be adjusted to optimize the acceptance of a selected mass range. The spectrometer has good acceptance for dimuons with $x_F > 0$ and p_T up to 3 GeV/c.

To design a spectrometer suitable for 50 GeV proton beam, it is useful to consider some kinematics of the Drell-Yan process. Table 2.2 compares the total center-of-mass energy and the Lorentz factor for proton beams of 50 GeV (at the present project), 120 GeV (at Fermilab Main Injector) and 800 GeV (at Fermilab Tevatron).

Table 2.2: The center-of-mass energy and the Lorentz factor for three beam energies

	50 GeV	120 GeV	800 GeV
$\sqrt{s}$	9.865 GeV	15.12 GeV	38.79 GeV
γ_f	5.259	7.998	20.65

The Lorentz factor of the nucleon-nucleon center-of-mass frame is

$$\gamma_f = \frac{E_1 + m_2}{\sqrt{s}}. \tag{2.13}$$

For μ^+ and μ^- emitted at 90° in the nucleon-nucleon center-of-mass frame and for $x_F \approx 0$, the opening angle θ of the two muons in the laboratory frame is expressed as

$$\tan(\theta/2) = \frac{1}{\gamma_f}. \tag{2.14}$$

For muons emitted at 90° in the virtual-photon rest frame, the laboratory kinematics of the muons largely depends on M and x_2 and does not depend on beam energy (or $\sqrt{s}$). More specifically,

$$p_\perp^{lab} = M/2. \tag{2.15}$$

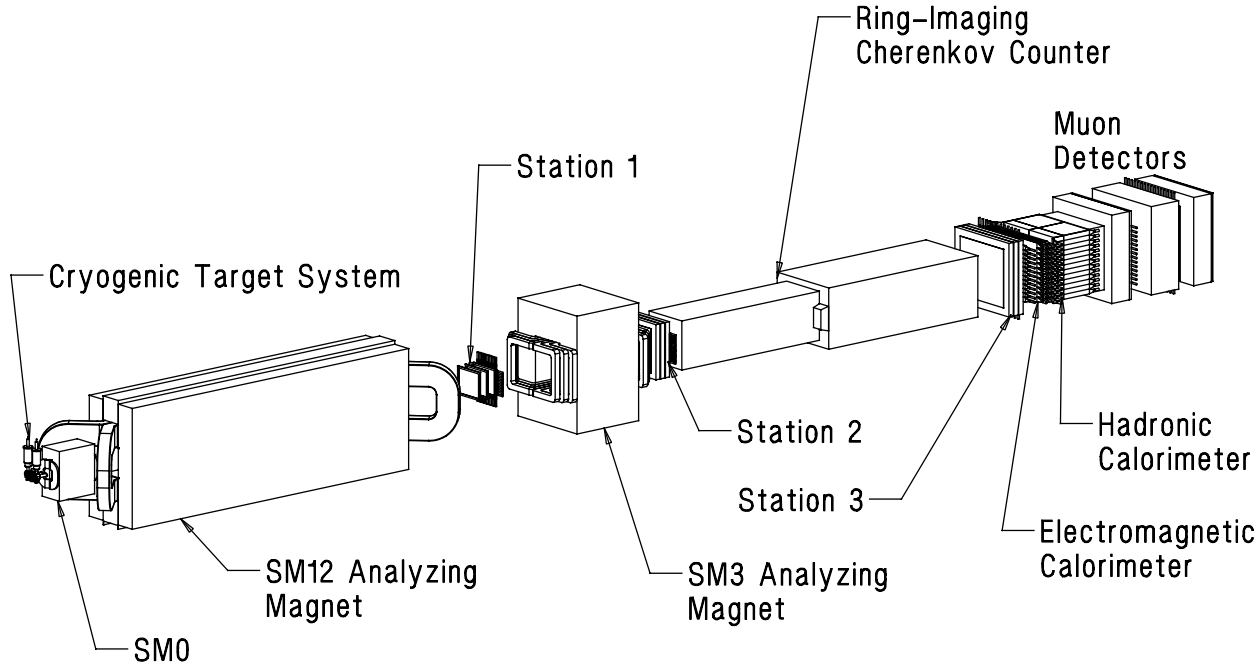

Figure 2.22: Schematic layout of the Meson-East focusing spectrometer at Fermilab.

$$p_{\parallel}^{lab} = \frac{1}{2} p_{\parallel}^{\gamma,lab} \simeq \frac{1}{2} x_1 p^{beam} \simeq \frac{x_1 s}{4 m_N} = \frac{M^2}{2 x_2 m_N}. \tag{2.16}$$

The measurable p_t range of muons should be almost the same as the E866 spectrometer or slightly smaller because the mass ($M_{\mu^+\mu^-}$) range interested is the same or slightly less. Thus the total magnetic rigidity ($\int Bdl$) of the magnets should be about 7 to 10 T·m, though it depends on the geometrical layout of the detectors. The P906 spectrometer has a magnetic rigidity of 8 T·m.

According to Eq. 2.14, the opening angle of the muons at 50 GeV is about 4 times larger than at 800 GeV (E866), and 1.5 times larger than at 120 GeV (P906). One idea to design the 50-GeV spectrometer is just to shorten the existing setup in the beam (z) direction with the factor of γ(50 GeV)/γ(800 GeV) or γ(50 GeV)/γ(120 GeV). However, since the maximum field strength of the P906 magnet is already near the saturation point, a magnet of almost the same length and wider aperture need to be considered.

Figure 2.23 shows the horizontal and vertical view of the proposed spectrometer. The target is assumed to be a liquid hydrogen or deuterium target 20-inch long and 3-inch wide. The produced charged particles are analyzed by a vertical-bending magnet, which is basically the same as the P906 magnet but has a wider aperture. The length of the magnet along the beam axis is 480.06 cm. The horizontal gap of the magnet at the exit is 116.84 cm and the vertical gap at the exit is 279.4 cm. The total momentum kick by this magnet is about 2.5 GeV/c. The incident proton beam is stopped by a copper beam dump, followed by a set of absorber materials. The second magnet and detectors are placed after the first magnet. The momentum kick by the second magnet is 0.5 GeV/c. The total length of the spectrometer system from the entrance of the first magnet to the end of the detector system is 1474.47 cm. The muons which hit all the detectors are accepted as signals.

A fast Monte-Carlo code, which takes into account the Drell-Yan cross section and the spectrometer configuration, has been used to estimate a statistical error for $\sigma(pd)/2\sigma(pp)$ shown

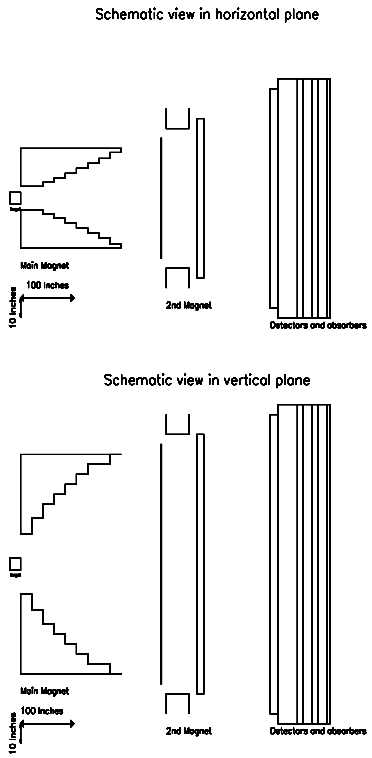

Figure 2.23: A schematic view of the prototype spectrometer. The top is the horizontal view and the bottom is the vertical view.

in Figure 2.13. In order to estimate the yields and statistical errors, the following assumptions have been applied:

- The beam intensity is 1×10^{12} protons/(3 sec.).
- The net efficiency of data acquisition is 0.5.
- Data are taken for 60 days each for 50-cm long proton and deuteron targets.

The performance of the spectrometer for $\vec{p}+\vec{p}$ measurement, nuclear dependence study of Drell-Yan, and J/Ψ production, has also been simulated and the results have been presented in the previous Section.

2.2.4 Summary

We present a broad range of physics topics which can be pursued at the 50-GeV PS using a dimuon spectrometer and a primary proton beam of 10^{12} per spill. The expected sensitivities of various measurments have been simulated for a preliminary design of the dimuon spectrometer. The physics scope can be considerably enlarged with the addition of polarized proton beam and with heavy-ion beams. More detailed studies using GEANT-based simulation are in progress to address the issues of background and to optimize the design of the spectrometer. Based on our study thus far, it is clear that a rich physics program can be mounted using the primary proton beam at the 50-GeV PS.

2.3 Multifragmentation

2.3.1 Introduction

In recent years, the extraction of the equation-of-state for nuclear matter and the confirmation of the liquid-gas phase transition in nuclear systems have been a major motivation in the search for and the study of simultaneous multi-fragment decays of heavy nuclei. Multifragmentation is a multiple production of intermediate mass fragments (IMFs; Z≥3), and has been theoretically prediced as a dominant disintegration mode of heavy nuclei at excitation energies near to the binding energy of nuclei and at nuclear densities well below the normal density of nuclear matter. Since this high excitation and low-density region well overlap with the liquid-gas coexistence region predicted for nuclear matter, systematic studies on multifragmentation might lead to the establishment of a liquid-gas phase transition in nulear systems.

In practise, the experimental quests for a nuclear liquid-gas phase transition have always faced some difficulties arising from the finiteness of excited nuclei, the non-zero charge of nuclei, the absence of external pressure to maintain the volume of a nuclear system at a given equilibrium condition, and so on. Despite such difficulties, recently, the ALADIN collaboration at GSI has successfully obtained a caloric curve of nuclei from a simultaneous measurement of the temperature and the excitation energy for excited projectile spectators in ^{197}Au+^{197}Au collisions at 600 MeV/nucleon[115]. It showed a qualitative similarity to the caloric curve of water: first-order phase transitions in macroscopic systems. This result attracted people's attentions towards multifragmentation and the nuclear phase transition. Several other experimental groups, however, have reported caloric curves without showing any phase transition behavior. Therefore, it is still premature to conclude that one can see the nuclear liquid-gas phase transition.

2.3.2 Experiment at KEK-PS (E337/393)

Aiming to extract a phase diagram and/or a caloric curve for nuclear matter, our group has also performed a series of experiments on target multifragmentation using light particle beams provided by the KEK 12-GeV Proton Synchrotron (KEK-PS) during the last several years. We chose light projectile-induced reactions because there are several advantages of using them over using heavy ion induced reactions[116, 117].

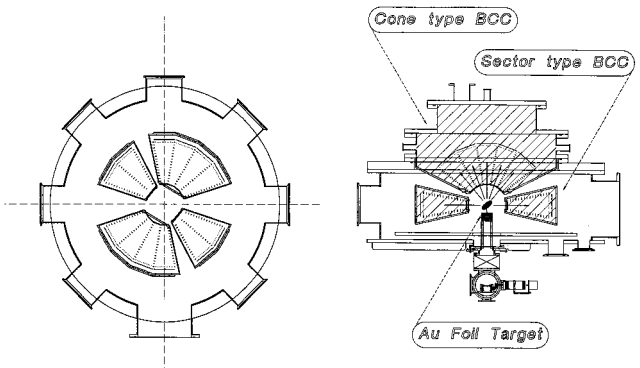

Figure 2.24: Schematic view of a new experimental setup with 37 BCCs.

Since we want to examine the nature of hot nuclei just before decay into multi-fragments, we have to measure as many fragments as possible. For such a purpose, we have developed a large acceptance Bragg Curve Counter (BCC[118]) array which consists of 25 BCCs enclosed in

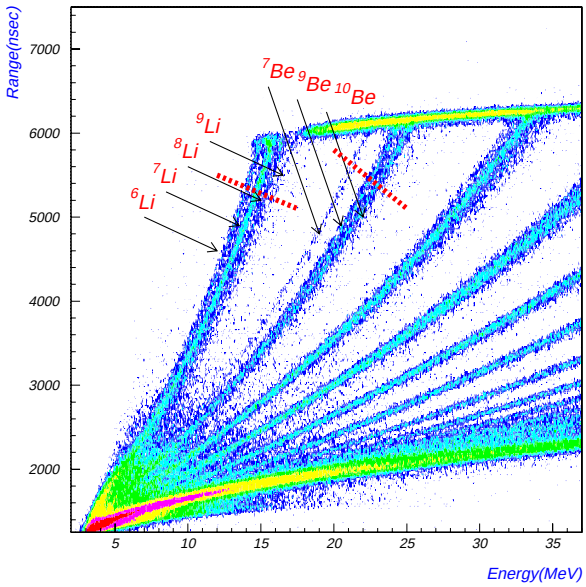

Figure 2.25: Typical isotope separation using a Bragg curve counter.

a single gas vessel and can cover nearly 13% of the entire solid angle. Twelve additional BCCs in a common horizontal plane including the target were used to measure the detailed angular distributions. In total, 37 BCCs covered about 20% of 4π(see Fig. 2.24).

The experiments were performed at the KEK-PS EP1-B and EP2-P1 lines. The typical intensity of primary 12- and 8-GeV proton beams focused onto the target was about 1×10^{9} particles per second with a beam spot size of approximately 5 mm in diameter. The targets used were self-supporting metallic Au and Ag and evaporated Tm and Sm onto 0.9 μm thick Mylar backing. The typical thickness of these targets was about 600 μg/cm^2, which was dectated by the energy-loss of IMFs in targets. The data were taken under the minimum bias condition, i.e. a sum of 37 self triggers from individual BCC.

A sample of range vs. kinetic energy scatter plot of IMFs detected by one of the 37 BCCs is shown in Fig. 2.25. Clear separation of lithium and beryllium isotopes was achieved by the BCC system. From the experimental information on the angular correlations among the IMFs and angular distributions of isotope temperature as well as energy spectra, a charge distribution, and the angular distributions of the IMFs with and without multiplicity gate were obtained. Typical energy spectra of Na fragments at E_p=12 GeV from 12 in-plane BCCs are shown in Fig. 2.26 sorted according to the associated IMF multiplicity.

The energy spectra for all IMFs at E_p=12 and 8 GeV showed the usual Maxwell-Boltzmann distribution-like shapes. It is possible to fit an individual spectrum by using a "moving source model"[119] with temperature parameters of 8-15 MeV, but it is almost impossible to fit all spectra at all angles simultaneously. The usual moving source model persistently underestimates the yields near to 70° in the laboratory system. The existence of this excess can be clearly demonstrated in the IMF angular distributions sorted according to the associated IMF multiplicity, as shown in Fig. 2.27 for the data at E_p=12 GeV. Against our expectation the 70° peaking feature remains, even after selecting IMF multiplicity=3 events. In other words, the 70° peaking component can not be enhanced by selecting high IMF multiplicity events. This fact might indicate that the 70° peaking component is generated in a rather wide range of impact parameters, suggesting thermal equilibrium at freeze-out is not completely achieved before the

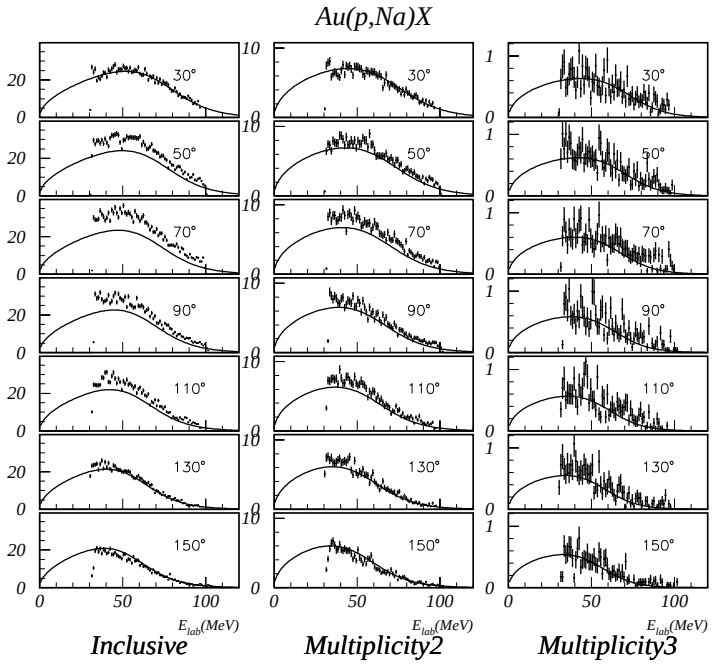

Figure 2.26: Energy spectra of Na isotope produced in Au+p reactions at E_p=12 GeV. The spectra were sorted according to the associated IMF multiplicity.

emission of IMFs. At E_p=8 GeV, we found that the 70° peaking feature is slightly weaker than at E_p=12 GeV.

More striking facts were revealed in the angular distributions of the isotope temperature obtained from the isotope yield ratios among lithium and beryllium isotopes. In figure 2.28, isotope temperatures at 12 GeV are shown as functions of the target mass, laboratory angle, and associated IMF multiplicity. For multiplicity=1 events, the isotope temperatures were about 4 MeV in the angle range between 50° and 130°, while 30° and 150° ones were as high as 10 MeV. For multiplicity=3 events, the isotope temperatures showed a strong target mass dependence, and were significantly higher than those for multiplicity=1 events. We can understand the latter feature naively because higher multiplicity events should correspond to more central and/or violent collisions. The temperature at 150° was extremely higher than the other angle data. From these facts we conclude that the thermal equilibrium at freeze-out realizes only locally in the IMF sources produced by 12-GeV proton induced reactions. At 8-GeV, the isotope temperatures are about 4 MeV at all angles between 30° and 150°, and show neither an IMF multiplicity dependence nor a target mass dependence. By plotting the isotope temperature as a function of the power-law index for the measured charge distribution of IMFs, which should be strongly correlated with the excitation energy of the emission source, we preliminarily obtained a "caloric curve" like figure which is quite similar to that obtained by the ALADIN collaboration. Our results seem to confirm the existence of the nuclear liquid-gas phase transition observed by the ALADIN collaboration, but clearly more work must be done before drawing any definite conclusions from this kind of analysis.

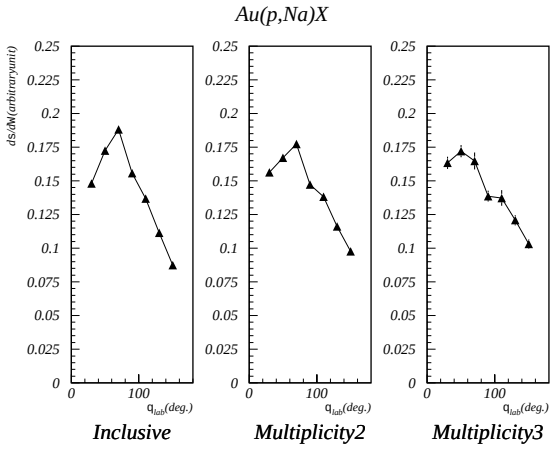

Figure 2.27: Angular distributions of Na isotope from Au+p reactions at E_p=12 GeV. Data were sorted according to the associated IMF multiplicity.

2.3.3 Experiment at the 50-GeV PS

We propose to measure target multifragmentation reactions induced by 5-30 GeV energy hadron beams from the 50-GeV PS as an extension of the present KEK-PS E337/393 experiment towards a much higher and lower incident energy domain in order to map out a large area of the nuclear phase diagram. By searching for signatures of critical phenomena for finite nuclear systems from multifragmentation data at various incident energies, we should be able to extract information on the thermodynamical aspect of the hot and/or dense nuclear matter, namely caloric curve, and to understand the origin of the sideward peaking angular distribution for IMFs.

Requirements on beams and the beam line

In order to use the proposed 50-GeV PS for the multifragmentation experiments, there are several requirements on the accelerator and the "primary" beam line. Since incident beam energies suitable for multifragmentation experiments are from 5 to 30 GeV, and since the most of exotic phenomena which might be related to the liquid-gas phase transition in the nuclear matter have been observed as a function of the incident beam energies, the incident energy of the beam should be variable. However, the required beam intensity for multifragmentation experiments is rather low, several 10^9 pps. Therefore, it would be possible to perform experiments using secondary beams produced from a high-intensity primary beam of about 10^{14}pps. In such a case, it is also easy to change the incident beam energy and the incident particle from proton to other hatrons, such as deuteron, antiproton, and pion by only adjusting the settings of the secondary beam line. By changing the incident particle we expect to be able to control the time scale required for energy transfer from the beam to the target nucleus and the total amount of the energy transfer. In order to use secondary beams for multifragmentation experiments, however, it it necessary to install an electrostatic or RF separator for high-energy secondary particles. The beam spot size should be as small as a few mm and a beam dump has to be located far away from the scattering chamber to reduce possible background from it.

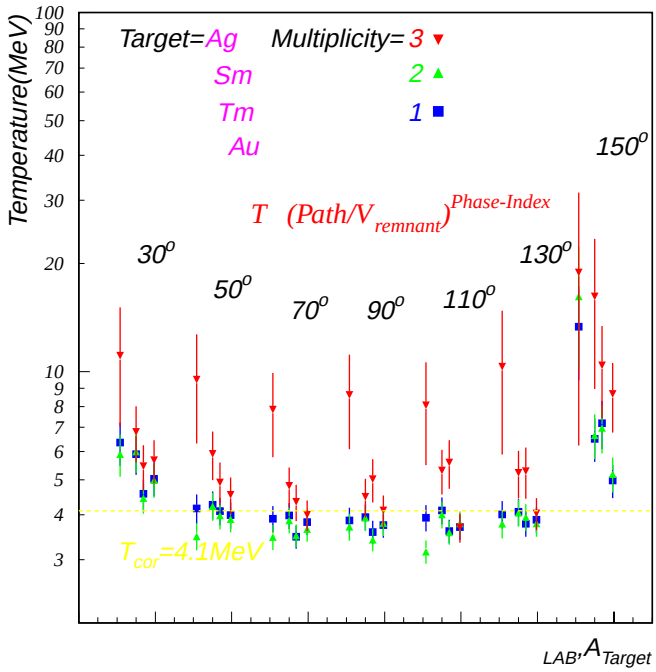

Figure 2.28: Nuclear temperatures as functions of the target mass and laboratory angle. They are sorted according to the associated IMF multiplicity.

Strategy

In the first phase we would use the E337/393 BCC array with minor modifications. We will mainly investigate the origin of the sideward peaking angular distribution for IMFs. We want to add a new multiplicity array that consists of fiber scintillators of very thin plastic scintillators in order to obtain a better 4π coverage.

In the second phase we are going to construct a new detector system which is capable of determining the energy deposition from the beam to the target. We are now investigating several candidates for such a detector system.

If light heavy-ion beams up to Si will be accelerated by the 50-GeV PS in the future, we would proceed in our quest of the equation-of-state (EOS) for nuclear matter at a high nuclear density domain by using them. Again, it is important that the beam energy be variable for multifragmentation reactions.

2.4 Strangeness nuclear physics with high-energy heavy-ion beams

2.4.1 Introduction

Considerable progress in the investigation of nuclear matter with strangeness and of interactions among baryons including hyperons has been made in the last ten years thanks to advanced experimental studies of hypernuclei and hyperon scattering at KEK 12-GeV PS and BNL AGS. A hypernucleus is a nucleus which possesses a strangeness quantum number. It is a hadronic many-body system that bounds not only nucleons, but also (a) hyperons, and thus it can be further said it is a quark system that contains (an) s quarks in it. Through the study of hypernuclei, new structure of hadronic bound systems will be revealed, since the interactions between hyperon-nucleon and hyperon-hyperon have unique features not realized in nucleon-only(u,d quarks only) system. In addition, the baryon-baryon interactions can be better investigated from a more general perspective, having information on the structure of hypernuclei. Studies of nuclear matter with multiple-strangeness should be crucial to establish an equation of state (EOS) of nuclear matter and interactions between nucleons and hyperons. Information on hyperon-nucleon and hyperon-hyperon interactions is indispensable in order to describe hadron interactions seamlessly in a framework of flavor SU(3).

Furthermore, hypernuclei provide a playground which is unique for investigating weak decay in hadronic many-body system. Λ hypernuclei eventually decay through a weak interaction from its ground state where a hyperon is deeply bound in the s orbital of a nucleus. The weak-decay process in a nucleus is totally different from those in free space, and gives us key imforamation in studying baryon-baryon weak interactions, such as $\Lambda + N \rightarrow N + N$.

One of the most critical measurements in strangeness physics is the one for hypernuclear magnetic moments, since the magnetic moment should be sensitive to the wave function of a Λ hyperon in a nucleus and surrounding nucleons. However, experiments that involve the measurement of particles from weak decay suffer from short lifetimes of the order of 10^{-12} sec. Although, various ideas on the measurement of a Λ hypernuclear magnetic moment have been proposed, no experiments have been performed until now due to the difficulty associated with the short lifetimes.

If high-energy heavy-ion beams are used, a new pathway toward precision measurements of hypernuclear magnetic moments opens. In the reaction, hypernuclei can be produced in the frame moving with the relativistic velocity, and their lifetimes become considerably longer by the γ factor. It thus becomes feasible to measure the magnetic moments, as described in the following sections. Once relativistic hypernuclei are obtained, it may also become possible to conduct experiments with inverse kinematics, such as by measuring the interaction cross sections, or even the pickup cross sections.

Strangeness nuclear physics is one of the central issues in the 50-GeV project. This letter aims to present another unique approach for investigating hypernuclei and strange nuclear matter, complimentary to those proposals utilizing secondary meson beams. In the following, we lay special emphasis on a measurement of the Λ hypernuclear magnetic moment, with an intention to demonstrate the feasibility of the experiments and to present a conceptual design of a possible experimental setup. The setup also allows us to further extend the experiments to multi-strangeness matter, such as double Λ hypernuclei, and to search for strange quark and hadronic matter in a relativistically moving frame.

2.4.2 Hypernuclei and hadronic matter in a relativistically moving frame

In high-energy heavy-ion collisions, it is well known that the participant-spectator model explains the general feature of the reaction, as illustrated in Fig. 2.29. Collisions between nuclei

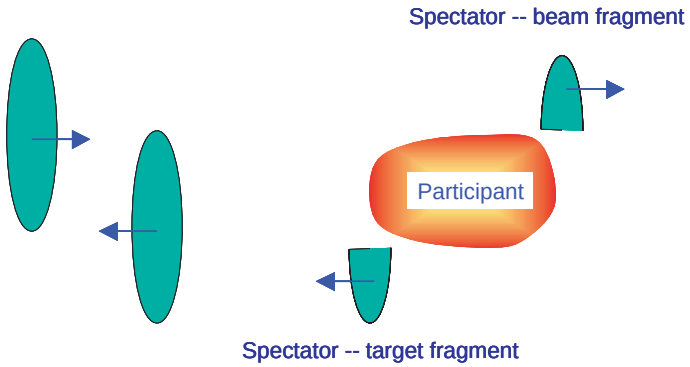

Figure 2.29: Participant-spectator model; a general feature of high-energy heavy-ion collisions.

are governed by the geometry of the colliding system, and only the nucleons in the overlapped region(participants) participate in the collision, while the nucleons in the off-overlapping region(spectators) pass through each other without experiencing a large disturbance. Hyperons, such as Λ, are produced in the participant region centered at the mid-rapidity via associate productions with relatively small Q-values. Those hyperons having relative momentum within the Fermi momentum of the projectile are possibly trapped by them and form a hypernucleus which has a relativistic velocity similar to that of the projectile fragment.

Value of relativistic hypernuclei

Until now, most hypernuclear physics experiments have been carried out using meson beams, such as pions and kaons. In such reactions, hypernuclei are produced at the target rapidity. The short lifetimes of Λ hypernuclei, which is around 200 ps, impose difficulty on these measurements, that require the detection of particles emitted in weak decay. On the contrary, hypernuclei are produced at the mid and projectile rapidity with heavy-ion beams whose energy is high enough to create hyperons abundantly. Although the difficulty is greatly eased, the difficulty of identifying hypernuclei from the large background of projectile fragments arizes.

The 50-GeV proton synchrotron accelerates heavy-ions to 25 GeV/nucleon for those ions with Z/A = 0.5. The γ factor for such heavy ions is 27.6, and the mean decay length($\beta\gamma c\tau$) of a Λ hyperon is as long as 218 cm, $c\tau$ for a Λ hyperon, being 7 cm. Λ hypernuclei at the projectile rapidity are expected to have a similar decay length, since the lifetimes of Λ hypernuclei are only slightly shorter than the free value, because the hypernuclear lifetimes were recently measured over a wide mass range.[121] The mean decay length of the Λ hypernuclei produced by the 25-GeV/nucleon beam is considerably longer than those available at BNL-AGS(15 GeV/nucleon) and KEK 12-GeV PS(6 GeV/nucleon), and is much more suitable for the production of hypernuclear beams. Thus, precision measurements of not only the Λ hypernuclear magnetic moments, but also the lifetimes, can be performed free from systematic errors inherent to the hypernuclear weak decay in the laboratory frame. Furthermore, hypernuclei with S=-2 can also be studied experimentally at projectile rapidity. It should be particularly noted that nuclei with strangeness greater than S=-2 can be investigated only by the heavy-ion reactions, but not by meson beams or electron beams. Thus, high-energy heavy-ion reactions will play a unique and essential role in the experimental investigation of future strangeness nuclear physics.

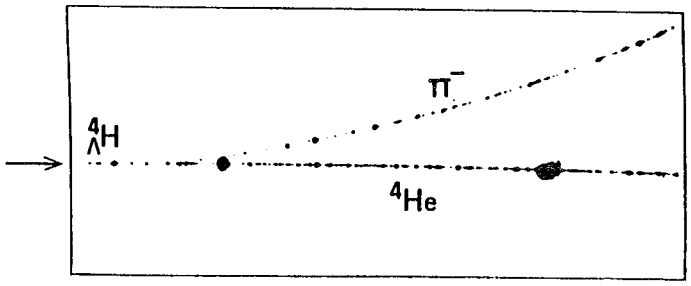

Figure 2.30: π mesonic weak decay of a relativistic ${}^{4}_{\Lambda}$H hypernucleus observed in the streamer chamber.[123]

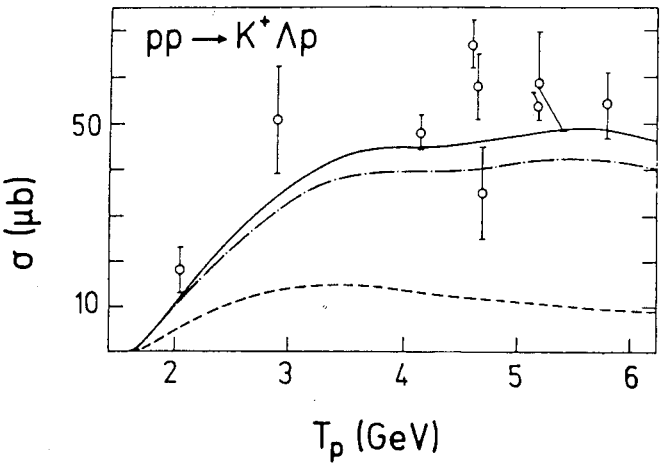

Figure 2.31: Cross section of the pp $\rightarrow$ $K^+\Lambda$p reaction as a function of the incident proton energy.

Previous study of relativistic Λ hypernuclei

The first observation of relativistic Λ hypernuclei produced in high-energy heavy-ion collisions was reported by an Arizona group.[122] The experiment was carried out at Bevalac using a 2.1-GeV/nucleon ^{16}O beam. It was claimed that the lifetime of A=16 Λ hypernuclei and also the hypernuclear cross section were determined based on the distribution of 22 decay vertex points.

More recently, the Dubna group also observed 22 Λ hypernuclear decay events and deduced the lifetimes of ${}^{4}_{\Lambda}$H with a 3.7-GeV/nucleon ^{4}He beam.[123] A clean picture of the streamer chamber that shows the weak-decay vertex of ${}^{4}_{\Lambda}\mathrm{H} \rightarrow {}^{4}\mathrm{He} + \pi^-$ is presented in Fig.2.30. In the experiment, the hypernuclear production of ${}^{3}_{\Lambda}$H and ${}^{4}_{\Lambda}$H was also identified with 5.14-GeV/nucleon ^{3}He and 3.7-GeV/nucleon ^{6}Li beams. Although the experiments at LBL and Dubna could not accumulate good statistics, since streamer chambers were used in both experiments, they demonstrated the production of relativistic Λ hypernuclei at the beam rapidity and the detection of their weak decay in high-energy heavy-ion collisions.

The threshold of Λ hyperon production in the elementary process $N + N \rightarrow \Lambda + N + K^+$ is 1.6 GeV. Thus, heavy-ion beams with energies greater than a few GeV are required to produce

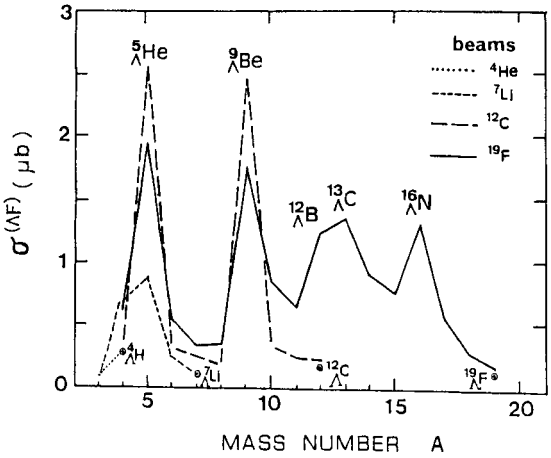

Figure 2.32: Λ hypernuclear production cross section by light nuclear beams at 3.7 and 3 GeV/nucleon.[124]

Λ hypernuclei. The beam energy dependence of $p + p \rightarrow p + \Lambda + K^+$ is shown in Fig.2.31, where the cross section rises from the threshold, and is almost constant (40-50 μb) in the energy range above 3 GeV.

Λ hypernuclear production by high-energy heavy-ion beams

Hypernuclear production by heavy-ion collisions were first theoretically studied by Bando *et. al.*[124] and later by Sano and Wakai[125] based on a coalescence model.

In their calculations, it was assumed that Λ hyperons are produced in the participant region, and that the hyperons and a projectile fragment coalesced with each other to form hypernuclei. The calculated Λ hypernuclear cross sections for various light Λ hypernuclei produced by ^{4}He, ^{7}Li, ^{12}C and ^{19}F heavy ion beams at 3.7 and 5.17 GeV/nucleon, which correspond to the Dubna beam energy, are shown in Fig.2.32.

Cross sections of the order of μb are expected for some of the Λ hypernuclei, and the calculations agreed well with the Dubna data, implying that the coalescence model explains the hypernuclear production mechanism fairly well.

Although hypernuclei were produced both in the projectile and central rapidity regions, the cross sections of single Λ hypernuclei are much greater in the projectile rapidity region, but double Λ hypernuclei are much greater in the central rapidity region.

The beam energy dependence of the Λ hypernuclear production was also studied by Sano and Wakai. At a beam energy higher than 10 GeV/nucleon, the secondary reaction, that is the (π^+,K$^+$) reaction, contributes to the hypernuclear cross section almost comparably to that of the primary reaction. The energy dependence of the cross section for the ^{12}C + ^{12}C $\rightarrow$ $^{6}_{\Lambda}$He + X is shown in Fig. 2.33 as an example.

S = -2 hypernuclei by high-energy heavy-ion collisions

The production cross sections of Ξ^- hypernuclei and double Λ hypernuclei were also calculated based on the coalescence model by Sano and Wakai for the Si + Au reaction at 14.5 GeV/nucleon, as shown in Table 2.4.2.[125] In the projectile rapidity region, the cross sections are small and

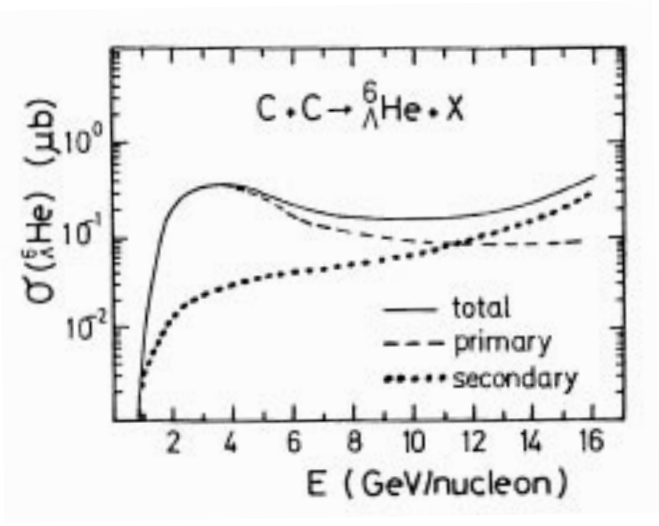

Figure 2.33: Projectile energy dependence of Λ hypernuclear production cross section at the beam rapidity for the C + C → ${}^{6}_{\Lambda}$He + X.[125]

around 1nb for Ξ^- hypernuclei and 1 pb for double Λ hypernuclei. However, the calculated cross sections are much larger in the central rapidity, where the P_T distribution of hypernuclei is expected to be greater than those in the projectile rapidity. However, a reasonable fraction of the total hypernuclear yield will be detected even for those hypernuclei produced in the mid-rapidity, provided a proper experimental setup is realized. In addition, hypernuclei may be better identified in this kinematical region, since it is free from background due to beam particles and projectile fragments.

Strange quark and hadronic matter

As briefly described in the previous section, studies of nuclear matter with multiple-strangeness should be crucial for our understanding of the interactions between hyperons and the equation of state (EOS) of nuclear matter in the flavor SU(3) regime.

Table 2.3: Cross sections of S=-2 hypernuclei calculated based on the coalescence model.[125]

Hypernucleus	peripheral collision σ(nb)	central collision $\sigma(\mu$b)
${}^{4}_{\Xi}$H	0.58	1.26
${}^{4}_{\Xi}$He	0.92	0.89
${}^{5}_{\Xi}$He	0.58	0.04
${}^{6}_{\Xi}$Li	0.58	2.2×10^{-3}
${}^{4}_{\Lambda\Lambda}$H	0.05×10^{-3}	1.26
${}^{5}_{\Lambda\Lambda}$H	0.11×10^{-3}	1.01
${}^{5}_{\Lambda\Lambda}$He	0.18×10^{-3}	0.71
${}^{6}_{\Lambda\Lambda}$Li	1.41×10^{-3}	0.03

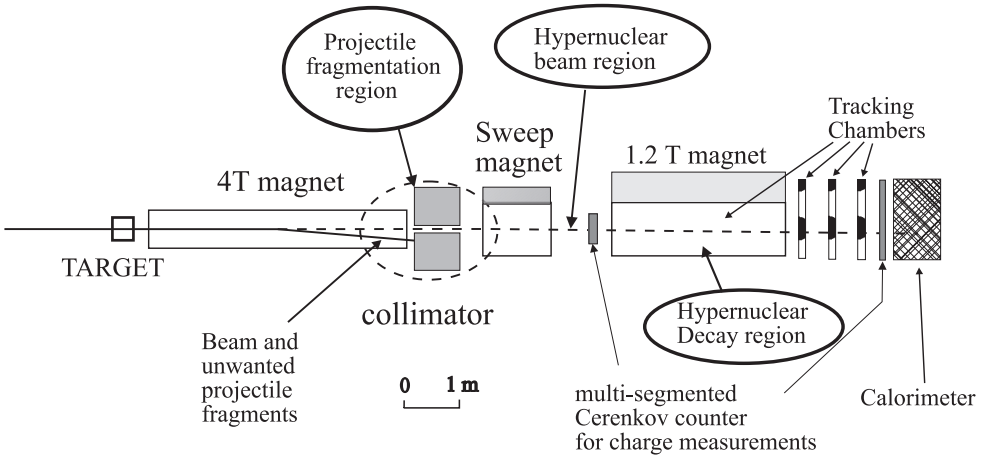

Figure 2.34: Conceptual setup for measuring Λ hypernuclear magnetic moments with the 25-GeV/nucleon projectile.

In the extreme of high strangeness contents, an exotic object called a strangelet may be created.[131] In an environment of a large baryon density where quarks are deconfined, the system may be more stable if some of u and d quarks are replaced by s quarks. There are trade-offs between the gain due to the Pauli principle and the loss due to the mass of strange quarks. When the chemical potential of the system is larger than the mass of the strange quark, the system favors to have a large fraction of strangeness, forming strange quark matter or a strangelet. There have been many experimental efforts to search for strangelets.[132] A recent intensive one among them was the E864 experiment at BNL-AGS. With 11.5-GeV/c/nucleon Au beams onto a Pb target, the E864 provided an upper limit (90% CL) to the strangelet production rate of 2-9 x 10^{-9} per 10% central Au + Pb collisions for positively/negatively/neutral charged strangelets.

2.4.3 Proposed conceptual experimental setup

In the following we discuss the conceptual experimental setup shown in Fig 2.34, by which a specific hypernucleus is identified and particles emitted in the weak decay are detected.

We assume the measurement of the ${}^{5}_{\Lambda}$He magnetic moment as a working example, since it is the most simple Λ hypernucleus with a configuration of $\alpha + \Lambda$, where the spin and isospin of the α particle are saturated.

In the case of Λ hypernuclei produced at the projectile rapidity of high-energy heavy-ion collisions, the direction and velocity of the hypernuclei are expected to be in a narrrow range. Therefore, large solid-angle coverage is not required to collect relativistic hypernuclear fragments. The most difficult part of the hypernuclear beam experiments is to identify a particular hypernucleus from the huge background of projectile-fragment and beam particles.

The cross sections of typical projectile fragments are known to be of the order of 1 barn, while the Λ hypernuclear cross sections are of the order of 1 μb. Thus, the ratio is given as

$$\sigma(\Lambda\ hypernucleus)/\sigma(Projectile\ fragment) = 10^{-5} - 10^{-6}.$$

In the first part of the setup, a strong magnetic field is applied to select a particular Λ hypernucleus of interest. With the 25-GeV/nucleon beam, the rigidity of projectile fragments and Λ hypernuclei at the beam rapidity is stiff. Thus, a large BL(Tesla $\cdot$ m) is required in

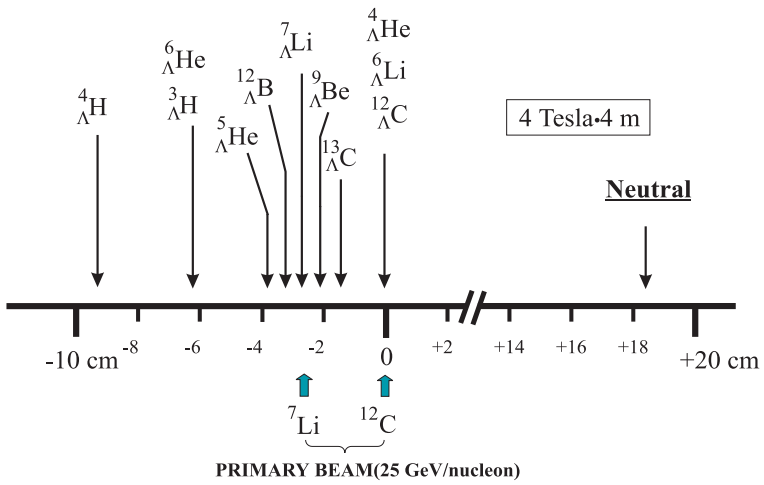

Figure 2.35: Separation of projectile fragments and hypernuclear fragments after the 4 Tesla·4 m separation region at 25 GeV/nucleon.

order to separate them from each other. Even with a 4 Tesla· 4m superconducting magnet, the separation between the beam and the relativistic Λ hypernuclei is minimal, and around a few cm at the exit of the magnet, as shown in Fig. 2.35

In the proposed setup, the beam particles and unwanted projectile fragments are stopped by a thick collimator, followed by a sweep magnet for the low-energy secondary particles. After the hypernuclear beam is selected, it is lead to the hypernuclear decay region where weak decay vertices are determined.

Yield estimate

In the following, we estimate the hypernuclear yield for the 25-GeV/nucleon ^{12}C + ^{12}C and 20-GeV/nucleon ^{7}Li + ^{12}C rections for the experimental setup shown in Fig. 2.34. The cross sections of the reactions were calculated by Wakai for these energies.[130] The cross section of $^{5}_{\Lambda}$He in the projectile rapidity is given as 0.2 and 0.37 μb for the 20-GeV/nucleon ^{7}Li + ^{12}C reaction and the 25-GeV/nucleon ^{12}C + ^{12}C reaction, respectively. We assume a typical cross section for $^{5}_{\Lambda}$He to be 0.1 μb in the following yield estimate. The beam intensity is assumed to be 10^{10}/spill (spill repetition = 3.4 s) and the target thickness 10 g/cm^2. In the projectile fragmentation region, $^{5}_{\Lambda}$He hypernuclei are selected by the collimator. The $^{5}_{\Lambda}$He hypernuclear beam then enters the weak-decay region where a 1.2 T magnetic field is applied perpendicular to the beam direction. Pions and protons emitted in the weak decay of hypernuclei are detected and their decay vertex points and momentum vectors are determined. In the case of $^{5}_{\Lambda}$He, the π^- decay branch is known to be relatively large, 0.44. The overall detection efficiency for the pion in the decay region is assumed to be 10%, although this is conservative. Then, the hypernuclear production rates, number of detected events and number of detected π-decay events are estimated as follows.

Although the estimated cross section depends on the detection efficiency of the weak decay particles, the event rate per day amounts up to 900, assuming a conservative efficiency of 0.1. The yield estimate is summarized in Table. 2.4.3

Table 2.4: Yield estimate of ${}^{5}_{\Lambda}$He hypernuclei and their weak decay events for the experimental setup shown in Fig. 2.34. The cross section and the beam intensity were assumed to be 0.1 μb and 10^{10} /spill, respectively.

Item	Rate per spill	Rate per day
Hypernuclear production rate	50	1.25×10^6
Hypernuclear events after the separation section	1.3	3.25×10^4
Hypernuclear decay events in the 2.2-m decay path	0.82	2.05×10^4
π mesonic weak decay rates($\Gamma_\pi/\Gamma_{total}$=0.44)	0.36	9.0×10^3
detected π-decay event(ε = 0.1)	0.036	9×10^2

2.4.4 Λ hypernuclear magnetic moment

The diagonal magnetic moment is one of the key observables in investigating the hypernuclear structure. Compared to ordinary nuclei, the Λ hypernuclear magnetic moment should be explained much more simply. It is free in the first order to the pion exchange current. Configuration-mixing effects on the Λ hypernuclear moments were studied by Tanaka[127], and it was found that they are generally small compared to that of ordinary nuclei, as expected because the isospin of a Λ hyperon is zero and the ΛN interaction is weak. Saito, Oka, and Suzuki investigated the effects of kaon and pion exchange currents to the magnetic moments of ${}^{5}_{\Lambda}$He and A=6 Λ hypernuclei.[126] It was suggested that ${}^{5}_{\Lambda}$He is a good place to look into an exotic effect. Since its magnetic moment should be well accounted for by the single-particle moment and that associated with the one-kaon exchange current, it is expected that the deviation from the calculated value, if any, can be attributed to exotic phenomena, such as those that require a quark degree of freedom. Takeuchi, Shimizu and Yazaki also discussed the contribution of the quark exchange currents to the magnetic moments based on a quark cluster model, presenting a possiblly large ($\sim$ -15%) effect for ${}^{4}_{\Sigma^-}$Li(1^+) and a small ($\sim$ -1%) effect for ${}^{4}_{\Lambda}$He(1^+).[128] For investigating hypernuclear magnetic moments, high-precision measurements better than a few % are required to differentiate exotic phenomena which are expected to manifest themselves when a Λ hyperon is embedded deeply inside a nucleus. In this regard, high-energy heavy-ion collisions, which have a potential to realize precision measurements of hypernuclear magnetic moments, have significance to hypernuclear investigations.

In the measurement of Λ hypernuclear moments, we will have to take the following 4 steps:

1. Identification of Λ hypernuclei
   — cleanly select hypernuclear events from the huge background of projectile fragments.

2. Lifetime measurements of light Λ hypernuclei
   — measure the distribution of decay the vertex points

3. Observation of polarized hypernuclei
   — optimize P_T for polarization and the hypernuclear yield

4. Observation of spin rotation through weak-decay pions
   — determine the precession frequency

Assuming that the Λ hypernuclear beam is well identified and that the weak decay have been measured, as described in the previous section, the most crucial issue is the polarization of the Λ hypernuclei. The polarization of Λ hypernuclei in heavy-ion collisions has never been

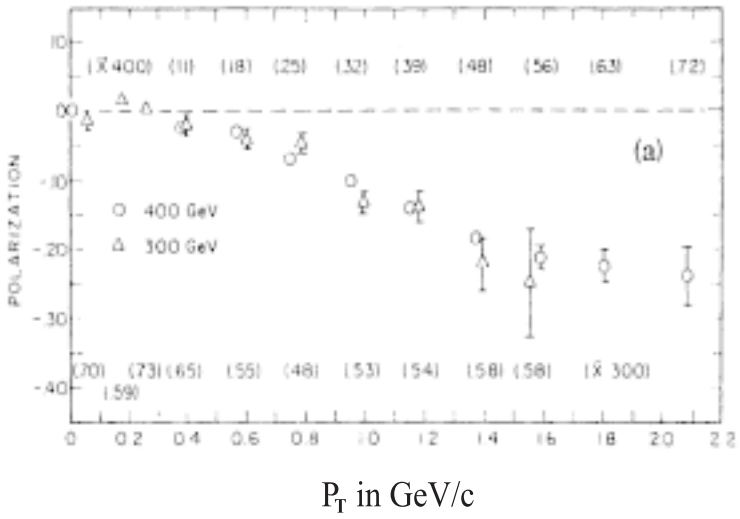

Figure 2.36: Transverse momentum dependence of Λ hyperon polarization by the p + Be reactions at 300, 400 GeV.[133]

observed experimetally. However, the polarization of a Λ hyperon formed in the quasifree region in high-energy proton reactions on nuclear targets has been well established. In this case, the degree of polarization was found not to be sensitive to the beam energy from 24 to 800 GeV, but to be linearly dependent on P_T, as shown in Fig. 2.36.[133] In the reaction of 400-GeV protons on a Be target, the polarization was measured to be P_Λ = -0.24 ± 0.04 at P_T = 2.1 GeV/c.

Furthermore, the polarization of a Λ hyperon in the quasifree region produced by the 1.8-GeV/nucleon Ar + KCl reaction also showed polarization, P_Λ = -0.10 ± 0.05, at $\langle P_T \rangle$ = 0.2 GeV.[134] From these data, it is expected that the Λ hypernuclei produced at finite P_T can also have some polarization. Sano and Wakai formulated the polarization of Λ hypernuclei within the framework of the coalescence model.[129] When a Λ hyperon is captured to the s orbit, the cross section will be expressed as

$$\sigma^{JM} \approx \sum_{M_\Lambda, M_F} \rho_\Lambda(M_\Lambda)\rho_F(M_F) < \frac{1}{2} J_F M_\Lambda M_F | JM >^2,$$

where J_F and J are the spins of the projectile fragment and the produced Λ hypernucleus, respectively. In the case of ${}^{5}_{\Lambda}$He, we expect that the polarization of the Λ hyperon is straightforwardedly transferred to the Λ hypernucleus, though this should be proved by experiments. It would be a cruicial step toward the determination of hypernuclear magnetic moments.

In order to derive the hypernuclear magnetic moment, the precession of the moment has to be observed. Since the angular distribution of pions emitted in the mesonic weak decay of Λ hypernuclei has asymmetry, measurements of the weak-decay pions along the trajectory readily give precession frequency, and therefore the magnetic moment. The magnetic moments of the Λ, Σ hyperons were measured in this way.[135] The total precession angle for the given mean decay length under a magnetic field of B is expressed as

$$\Delta\theta = 18.3 \cdot \frac{\mu_{HY}}{\mu_N} \cdot \int B dL$$

in units of degree, Tesla and m for $\Delta\theta, B$ and L. Since the mean decay length of hypernuclear fragments corresponding to the 25-GeV/nucleon projectile fragments is $L = \beta\gamma c\tau = 2.2m$, the

precession angle is given by

$$\Delta\theta = 40.3gB,$$

where g is the gyromagnetic ratio of the hypernucleus. When a magnetic field of 1.2 Tesla is applied in the hypernuclear decay region, the precession angle is $\Delta\theta$ = 29.6 degrees for the g factor of a free Λ hyperon, g_Λ = -0.6138. The large total precession angle and the number of π mesonic weak decay events detected in the decay region, as estimated in the previous subsection, make measurements of Λ hypernuclear magnetic moments quite promising.

2.4.5 Summary

We proposed to fully utilize high-energy heavy-ion reactions in order to explore strangeness nuclear physics in a completely new regime, that is in the relativistically moving frame, which is in contrast to those at the laboratory frame. Since the 50-GeV PS possibly provides 25-GeV/nucleon nuclear beams for A/Z = 2 heavy ions, Λ hypernuclei and other strangeness nuclear matter moving at relativistic velocity can b abundantlye produced. Thus, it will be possible to conduct a wide variety of experiments for strangeness nuclear physics, which cannot be realized by experiments with meson beams, and also by primary beams, such as electrons and protons. In this letter, we put particular emphasis on the production of hypernuclear beams and measurement of Λ hypernuclear magnetic moments. Such experiments become possible by taking full advantage of relativistic hypernuclei, which have a mean decay length of about 2.2 m at 25 GeV/nucleons. It was shown that a large number of Λ hypernuclei will be produced in the projectile rapidity, and that they can be idetified with a proposed conceptual setup. The precession of hypernuclear spin can be measured through the detection of pions from mesonic weak decay. The present proposal requires the acceleration of ions as heavy as at least ^{12}C and a beam intensity greater than 10^{10} per spill at the 50-GeV PS. With these heavy ion beams, a unique opportunity for strangeness nuclear physics will be explored and the dream experiment of measuring hypernuclear magnetic moments will be realized.

2.5 Systematic study of the collective behavior in hadron production

2.5.1 Introduction/motivation

Relativistic heavy ion collisions provide a unique tool for studying the nuclear properties at high temperature and density. Nuclear matter formed in high-energy heavy ion collisions is dense and energetic enough so that quarks are no longer confined to each individual nucleon, but move freely in a relatively large volume. This new phase of matter is called the quark gluon plasma (QGP). According to a lattice QCD calculation, the phase transition takes place at around 200 MeV of temperature.

Enthusiasm to create the QGP in the laboratory has initiated heavy-ion programs both at BNL-AGS, providing heavy ion beams at 12 - 15 AGeV, and at CERN-SPS, with beams at 160 - 200 AGeV. We have been actively involved in the heavy-ion programs at the AGS experiments (E802/E859/E866) and also at the SPS experiments (NA44/WA98)[136, 137]. A few years of pioneering experiments have revealed several interesting features of data, among which are the J/ψ suppression[139], the enhancement of low-mass lepton pair production[140], the enhancement of multistrage hyperons[141] and the collective behavior in hadron production. From global interpretations of the data, it is stated that a quark gluon plasma has been created in Pb+Pb collisions at an energy of 158 AGeV. Although there are criticisms against the claim of QGP formation at CERN-SPS, there are several experimental proofs/signatures that significant change in the reaction takes place in between the AGS and SPS energies. This is exactly the energy regime which the 50-GeV PS can provides.

In this letter, we first discuss the importance of the heavy-ion project at the 50-GeV PS by showing important trends/signatures found at the AGS and SPS. Namely, the change in the proton rapidity distributions in between the AGS and SPS, the reduction of the radial flow velocity from AGS to SPS, the change of sign in the elliptic flow pattern between AGS (below AGS) and SPS, followed by a plan for experiments.

2.5.2 Stopping power

In heavy-ion collisions at lower energies, it is expected that the colliding nuclei stop each other after violent nucleon-nucleon collisions, and form nuclear matter at high baryon density, while at higher energies, colliding nuclei rapidly pass through each other while forming baryon-free high-energy domains behind. The energy density and maximum baryon density are expected to change drastically between these high- and low-energy collisions. This issue is often called the stopping-power problem and is tightly related with the reaction dynamics and the equation of state of the fireball formed in the collisions.

The rapidity distribution of protons formed in central heavy ion collisions provides crucial information on the stopping. Figure 2.37 shows the proton rapidity distributions, comparing collisions of 1, 11 and 158 AGeV. The rapidity is scaled by the beam rapidity of collisions. There is a common trend of increasing width of the scaled rapidity distribution with increasing beam energies. It can be seen that there is a qualitative change of shape from the single-peak to the double-peak distribution in between 11 AGeV and 158 AGeV. This is the first hint of a significant change in collisions at the energy regime which the 50-GeV PS can provide. At this energy, we expect the highest baryon density achieved in the collisions.

2.5.3 Success of an expanding source model

Hadron production has been intensively studied at both the AGS and SPS energies. Not only the single particle spectra, but also the HBT two-particle correlations have been studied system-

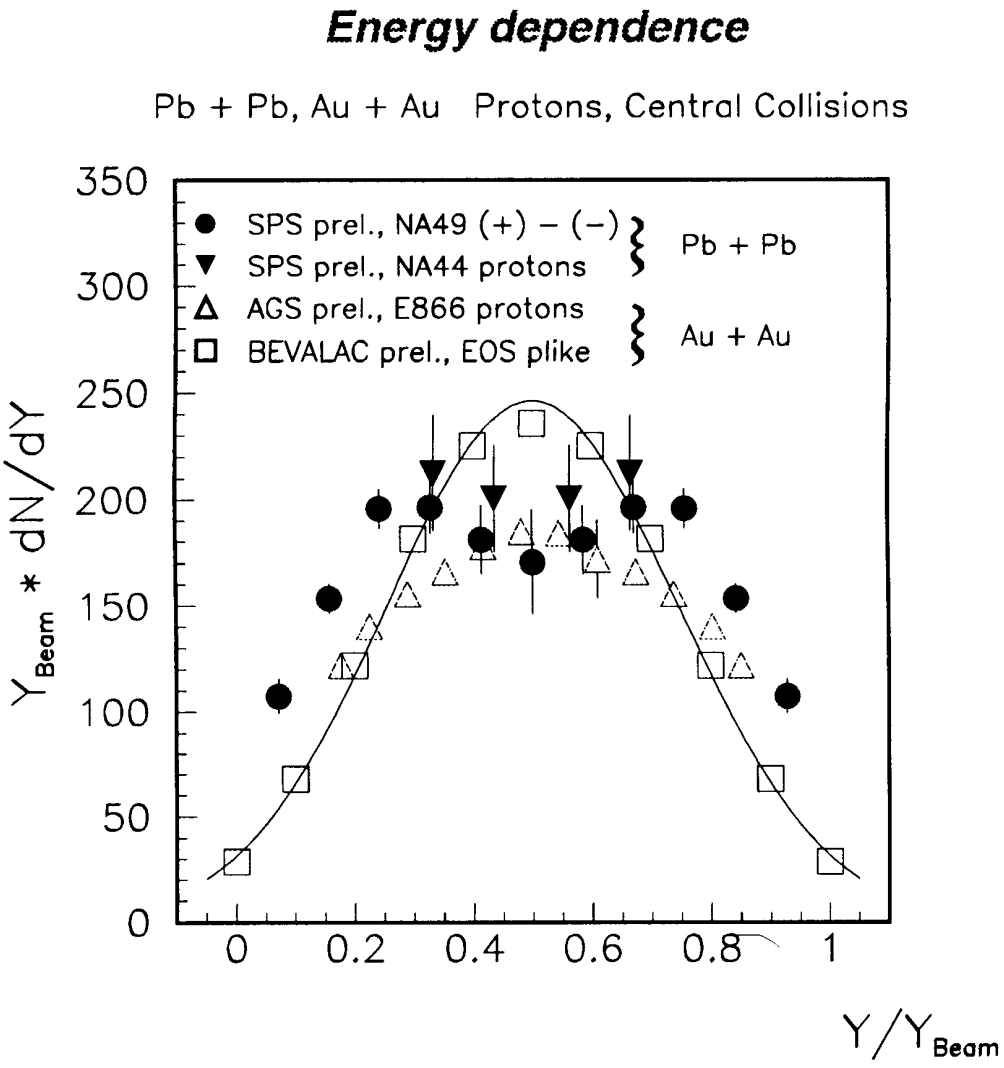

Figure 2.37: Proton rapidity distributions in 1, 11 and 158 A GeV central heavy-ion collisions.

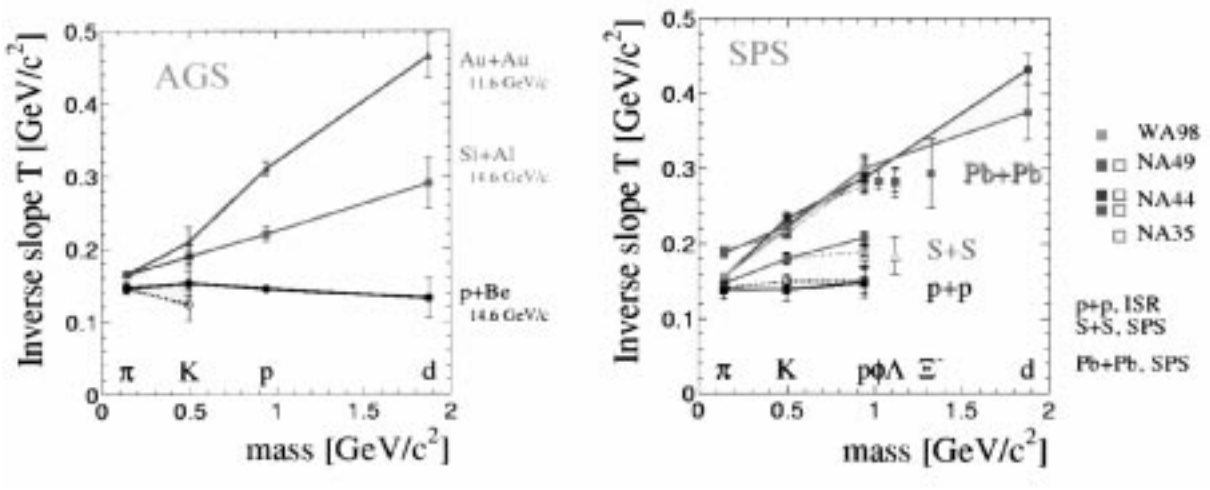

Figure 2.38: Inverse slope parameters as a function of the particle mass. The left panel is for collisions at AGS and the right panel for SPS.

atically. A study of the single-particle spectra reveals that the invariant differential cross section is exponential in mt, as is well known as "mt scaling" in pp or pA collisions. However, while in pp or pA the slope of the exponential is the same for all particle species; the inverse slope of the exponential distributions in AA is found to be proportional to the mass of the particles. This striking feature of the single-particle spectra in AA has been confirmed at both AGS and SPS, as shown in Fig. 2.38.

At AGS and SPS, the HBT two-particle correlations have been systematically studied with very high statistics, where interesting features are also seen. With the nature of HBT correlations, the correlation function depends on the relative momentum of the particles, and should be independent of the momentum sum of two partiles. However, a clear dependence of the correlation has been reported both at AGS and SPS.

Both features are attributed to the expanding source model[151], in which local thermal equilibrium and independent transverse and longitudinal motion are assumed. Motivated by these observations, that both the single particle spectra and the HBT two particle correlations are consistent with predictions of the expanding source model, simultaneous fits of both data using the same framework of the model have been successfully carried out both at AGS[150] and SPS[152] (Fig. 2.39). Thus, a precise temperature and transverse expansion velocity can be obtained. The beam energy dependence of the temperature and the transverse expansion velocity are shown in Fig. 2.40. As can be clearly seen in Fig. 2.40, as the beam energy increases, the temperature increases at collision energies of from a few AGeV to 158 AGeV collisions. The transverse expansion velocity also increases up to a beam energy of 10 AGeV, but seems to decrease from 10 A GeV to 158 A GeV. This is another hint of the significant change in between the AGS and SPS.

At the phase transition from ordinal matter to the QGP, the equation of state is expected to be "softened". At the critical temperature, the compressibility becomes small, exhibiting a softening due to the increased number of degrees of freedom[143]. The observed reduction of the transverse expansion can be attributed to the QGP formation in Pb+Pb collisions at 158 A GeV, which is supported by the recent observation of anomalous J/ψ suppression[139] and low-mass dilepton enhancement[140].

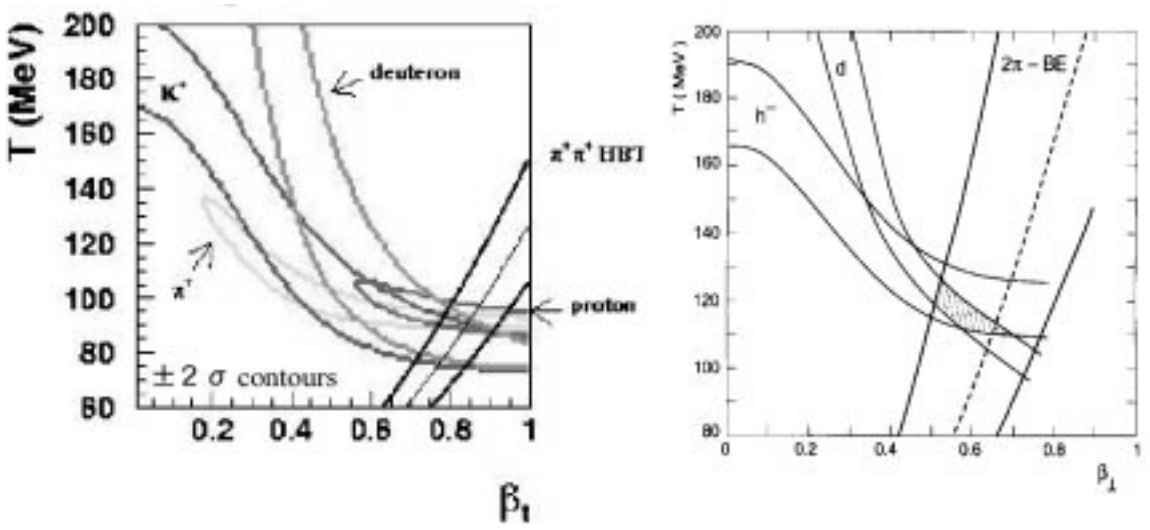

Figure 2.39: Allowed regions of temperature and the transverse expansion velocity derived from the single-particle spectra and the HBT two-particle correlations. The left panel is for AGS[150] and the right panel for SPS.

2.5.4 Collective flow

As demonstrated above, the collective feature of hadron production has been established both at AGS and SPS. Studies of the collective motion in the final state of the produced hadrons are expected to provide information on both the dynamics of heavy-ion collisions and the equation of state [142]. The observation of collective behavior in the system provides a validation of a hydrodynamical picture of hot and dense nuclear matter. Once a hydrodynamical interpretation is established, collective motion results from pressure gradients in the matter, which could reflect the compressibility of the underlying equation of state.

Recently, the importance of flow studies at ultra relativistic heavy ion collisions has been intensively discussed [143, 144, 145]. The effect of a phase transition on the collective flow has been demonstrated by a hydrodynamical calculation [143], as shown in Fig. 2.5.4. This calculation predicts the minimum collective flow at a beam energy corresponding to the threshold of the QGP formation. A significant difference in the collective flow with and without the QGP formation is shown with this calculation. Thus, a measurement of the excitation function at the energy region of the 50-GeV PS is crucially important.

Not only the isotropic transverse expansion discussed above, but also non-isotropic transverse flow, has been studied. Experimentally, the azimuthal distribution of particle emission is analyzed with respect to the reaction plane in terms of a Fourier expansion as

$$\frac{1}{N}\frac{dN}{d(\phi-\Phi_0)} = 1 + 2v_1\cos(\phi-\Phi_0) + 2v_2\cos(2(\phi-\Phi_0)), \tag{2.17}$$

where ϕ is the azimuthal angle of the particle and Φ_0 is the azimuthal angle of the reaction plane in the laboratory frame. The first two coefficients in the Fourier decomposition are termed directed and elliptic flow. Namely, v_1 quantifies the directed flow, whereas v_2 quantifies the elliptic flow.

A systematic study of directed flow and elliptic flow has been carried out. In Figure 2.5.4, the strength of the elliptic flow is compared. The v_2 values for protons, pions, and kaons near mid-rapidity are plotted as a function of the beam energy. One of the striking features is a change in the sign of the values of v_2. At lower energies, particles tend to be emitted preferentially

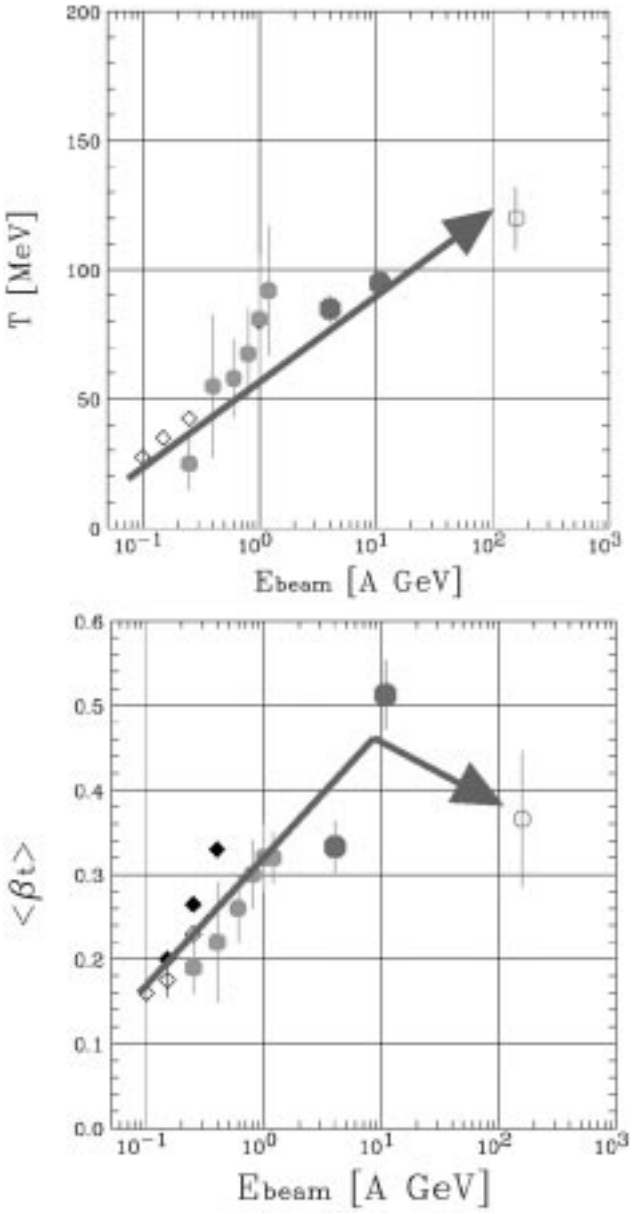

Figure 2.40: Beam energy dependence of the temperature and transverse expansion velocity [150]. Note that only the data points at 10 and 158 A GeV are obtained from the simultaneous fits explained in the text. All other points are from an analysis of the single-particle spectra alone.

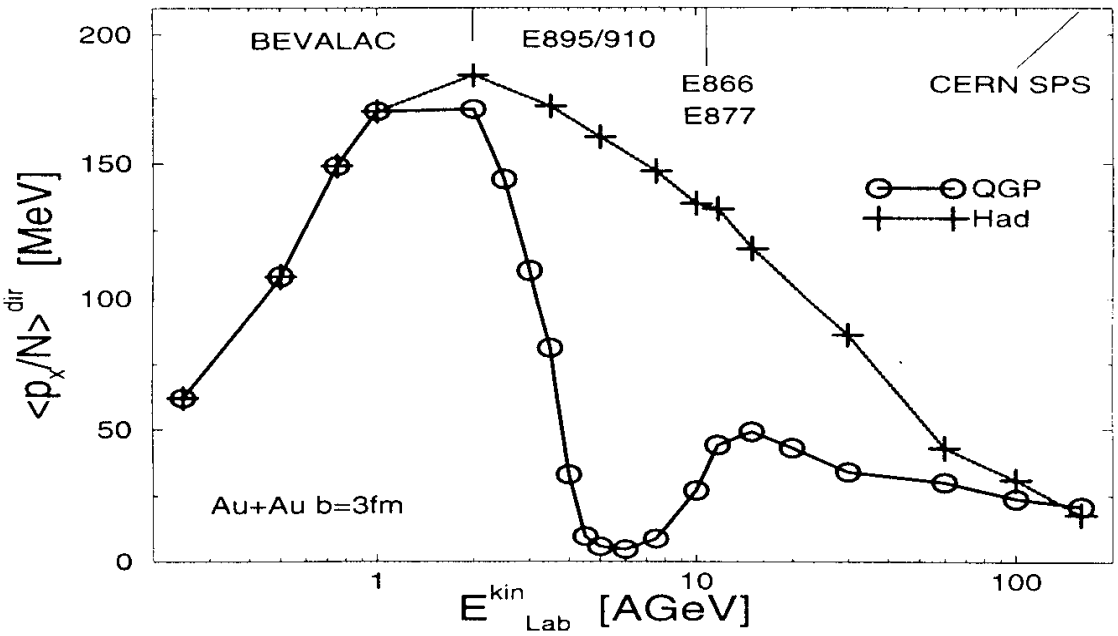

Figure 2.41: Excitation function of the strength of the collective flow, as calculated for 3+1 dimensional hydrodynamics for Au+Au collisions with an impact parameter of 3 fm [143].

perpendicular to the reaction plane, while at higher energies protons and pions are emitted in the reaction plane. This transition from out-of-plane to in-plane emission occurs at around 5-10 A GeV for both protons and pions. This is the third sign of a significant change between AGS and SPS.

A somewhat peculiar behaviour of K^+ has been observed, which may be attributed to the effect of the in-medium potential [147, 138]. The azimuthal distribution of a particular particle species in the final state is also expected to be sensitive to the in-medium potential of the particle, which is repulsive for K^+. An intuitive model calculation has shown that it is qualitatively consistent with this effect [148].

2.5.5 Proposed experiment at the 50-GeV PS

As discussed, the heavy-ion collisions at the energy of the 50-GeV PS corresponds to the maximum baryon density and change in the collisions dynamics or equation of state due to the possible formation of a quark gluon plasma. To establish a more quantitative description of the change between the AGS and the SPS, some type of experiment to measure an excitaion fuction is required.

Here, we would like to state our intention of a heavy-ion experiment at the 50-GeV PS to meet this requirement. We will establish an experiment with emphasis on the issues discussed above. The experiment will measure:

1. the single-particle spectra of positive and negative π,K,p and d, including Δ's;
2. two-particle correlations of positive and negative π's and K's and protons.

Furthermore, correlations of these observables will be studied with:

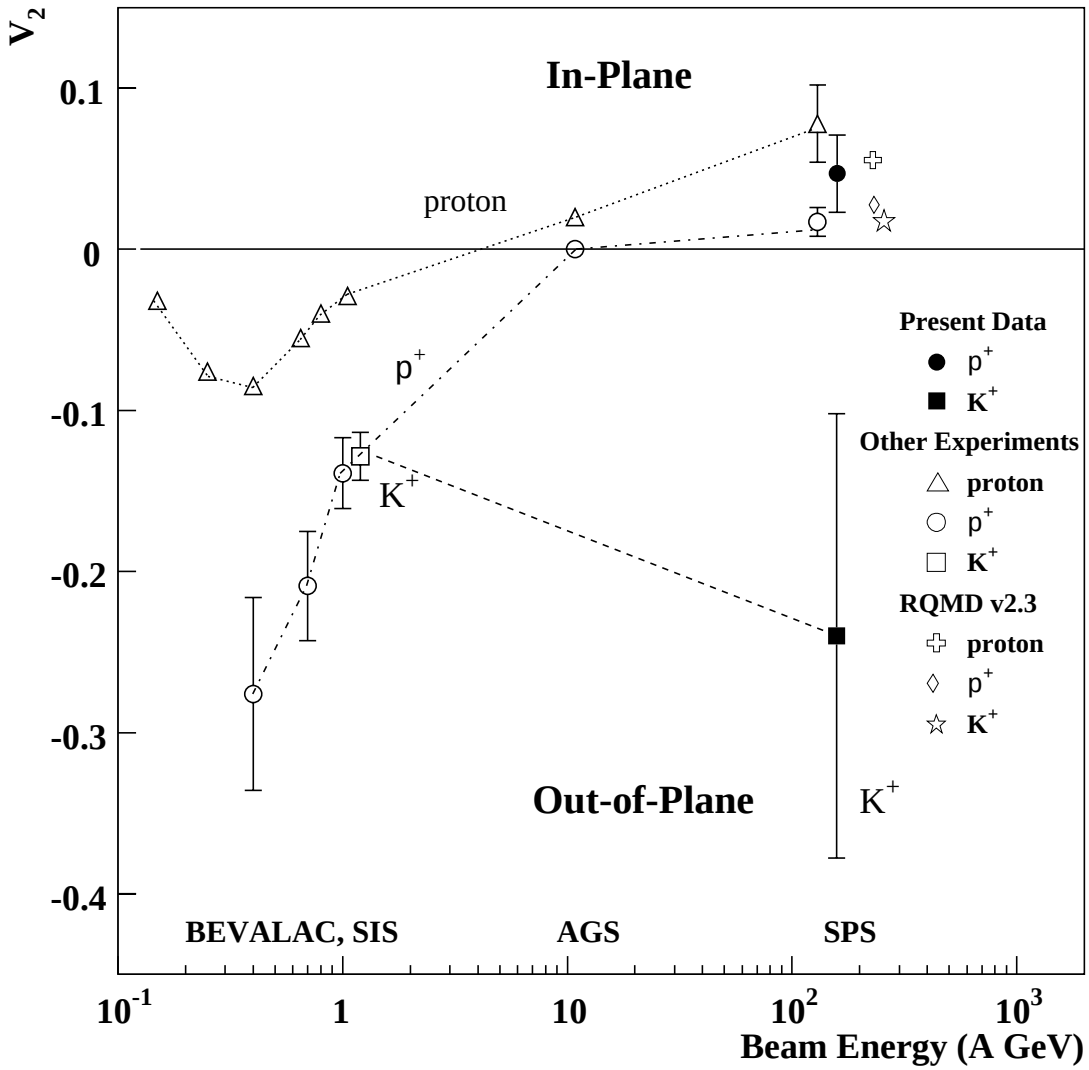

Figure 2.42: Beam energy dependence of the v_2 value near to the mid-rapidity [138]. RQMD (v2.3 cascade mode) calculations for proton, π^+ and K^+ in 158 A·GeV Pb + Pb collisions are also shown for the impact-parameter range $b = 6.5 - 12$ fm with a filter of the experimental acceptance.

1. the azimuthal direction of the reaction plane;

2. centrality of collisions;

3. beam energies and projectile and target nuclei systematics.

For such a measurement, a large-acceptance magnetic spectrometer with particle identification is required as a primary device. Conceptually, the magnetic spectrometer will be similar to what we had constructed at AGS and SPS. In addition, it is required to have event-characterizing detectors, which would provide not only the centrality of the collisions, but also information concerning the reaction plane, event by event. According to our experience at CERN-SPS, a plastic-ball detector with 2π coverage in azimuth at the target rapidity region is known to serve for the purposes. A hadronic calorimeter at the projectile rapidity region also works for the reaction plane determination. From the analysis of the azimuthal correlations, the azimuthal angle of the reaction plane can be determined. A preliminary Monte-Carlo calculation has shown that the current design of the plastic-ball detector provides an angular resolution of about 50 degrees in heavy ion collisions at this energy. The resolution can be improved in several ways. In particular, the simultaneous use of the plastic-ball detector and a hadronic calorimeter will improve the resolution significantly. Since the resolution of the reaction-plane determination is one of the key issues for this experiment in the sense of sesitivities and accuracies, we would like to place our effort on the R&D of this device.

The experiment will be carried out in several phases. In the first phase, measurements of the single particle spectra and HBT two-particle correlations will be carried out with lighter ion beams together with R&D work on the reaction-plane determination techniques. Particularly, the performance of a hadronic calorimeter will be investigated in terms of the angular resolution of the reaction plane. Finally, at the third stage, systematic measurements with the reaction-plane detectors will be carried out using truly heavy ion beams.

2.6 Polarized beam/target experiments

2.6.1 Introduction

In order to understand and establish quantum chromodynamics (QCD) in both the perturbative and non-perturbative region, spin physics plays an essential role. Establishing QCD, combining it with electro-weak theory, and making the experimentally tested unified model will be ultimate goals of the 50-GeV PS project.

In this letter, we discuss a spin asymmetry measurement of particle productions in the pp reaction. The single particles here mean $\rho, \phi, \pi^{\pm}, K^{0,\pm}$, and Λ.

As has often been seen in history, many simple hadron models based on quarks have turned out to be unrealistic, because they do not reproduce the spin observables, though they do reproduce the spin-independent properties. Spin observables provide a crucial test of hadron models.

In general, the spin dependence in the hadron reactions had been believed to become less significant at higher energy as the direct gluon contribution increases compared to the quark contribution. Also, the gluon was expected to be unpolarized, as was sea-quarks. However, the gluon is now one of the candidates for the spin carrier of the proton, since the proton spin puzzle appeared in 1987. Also, in the medium-energy region, hadron production in a proton-proton reaction is the place where models of quark rearrangement and quark confinement are built and tested. There, single and double spin asymmetries are essential to study the spin transfer of quarks from the beam and target protons to the produced hadrons. Indeed, a large spin asymmetry in particle productions has been observed in experiments at BNL-AGS, FNAL etc. The quark rearrangement and hadronization, together with the quark confinement mechanism, are the frontier of low-energy QCD.

For single spin asymmetry in the $\vec{p}p$ reaction, a polarised proton beam is essential, because an unpolarized proton beam on a polarized proton target cannot replace it. The reason is, it always contains contributions from the neutron and nuclei in the polarized target. A polarized pure hydrogen target does not yet exist, except for a gas target. The initial state needs to be well defined to be pp, which means the T=1 state or two sets of uud valence quarks.

2.6.2 Spin experiments with a primary proton beam: Wide-Acceptance Hadron Detector (WAHD)

Two types of the produced particles will be detected: short-lived particles which decay into two particles, such as ρ, ϕ, K^0, Λ, and long-lived particles, such as $\pi^{\pm}$, $K^{\pm}$.

The wide acceptance hadron detector (WAHD) is a main component for detecting these particles. Rather than simulations, we can refer to a detector system which is already working at the comparative energy region as the 50-GeV PS. It is the HERMES spectrometer at DESY-HERA. Because the beam energy is 27.5 GeV, the energy of the exchanged virtual photon in the scattering process, or the energy transfer to the target, ranges from 4 to 23 GeV. This is also the expected energy transfer to the target at the 50-GeV PS. Fig. 2.43 shows the vertical cross section of the HERMES spectrometer. The detector is split to the top half and the bottom half at the beam level. The angular acceptance in the vetical direction is $\pm$140mrad. Figs. 2.44 and 2.45 show the reconstructed ϕ and ρ mass from the $\phi \rightarrow K^+K^-$ and $\rho \rightarrow \pi^+\pi^-$ decays. K^0 is similarly measured from $\pi^+\pi^-$, and Λ from $p\pi$ decay provides Λ polarization, as it is weak decay.

The production of long-lived particles, such as $\pi^{\pm}$, $K^{\pm}$, $p(\bar{p})$, needs to be detected with good particle identification. This is now becoming technically feasible. The Ring Imaging Cherenkov Counter (RICH) of HERMES (Fig. 2.46) has been operational since 1998, and has shown that

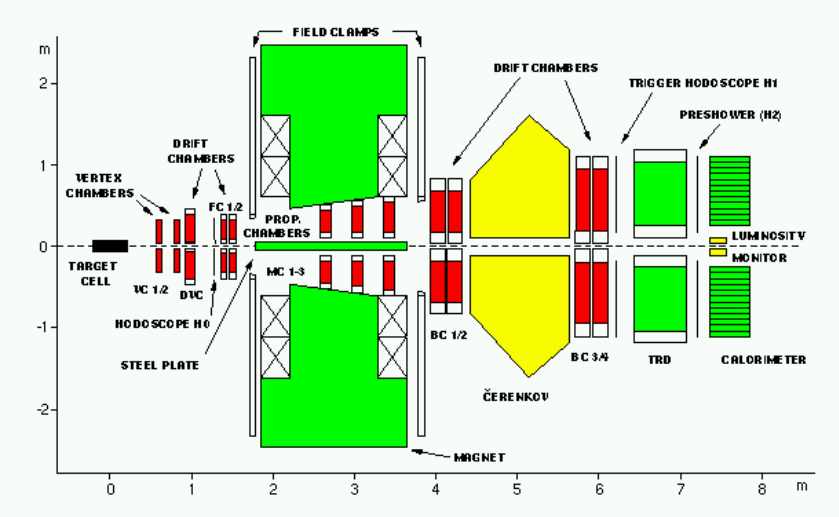

Figure 2.43: Vertical view of the HERMES spectrometer.

the identification of these particles is possible in the momentum range of 2 to 20 GeV/c, which is almost the total range which we would like to cover at the 50-GeV PS. The essential ingredient of HERMES-RICH was a dual radiator: silica aerogel and C_4F_{10} gas. The Cherenkov emission angle as a function of the momentum indicates the capability of particle identification, as shown in Fig. 2.47. Further development of the technique is expected.

The WAHD, which is suitable for the detection of both the decaying and non-decaying particles, is one of the key elements in the spin physics program at the 50-GeV PS.

2.6.3 Spin-asymmetry measurements

The single-spin asymmetry of particle production with a transverse polarized proton beam on a proton target is the first quantity to measure. The single-spin asymmetry in the production of $\pi^{\pm}$, $K^{\pm}$, K^0, ρ, and ϕ provides a set of information on how a quark becomes bound with an antiquark, in particular how the spin of the valence quark is coupled with the spin of the sea-quark. The combination of a psuedo-scalar meson and a vector meson data is useful to analyse this problem. An exception, in terms of the reaction mechanism, is the case of ϕ production, where an $s\bar{s}$ pair is produced. The asymmetry of ϕ production, if non-zero, suggests the propagation of polarization of a quark-antiquark pair which has annihilated prior to ϕ production.

It is essential to map the entire kinematic region of (x_F, p_T), except for the region where the particle in the target region is of too low momentum to detect. The contribution of the valence quark in the beam proton can be well monitored by the x_F dependence of the asymmetry.

Baryon production is also a subject to study. The production of Λ with a polarized proton beam, and a subsequent measurement of Λ polarization would allow us to determine the spin-transfer coefficient. How a Λ becomes polarized in the reaction is an unsettled problem to be studied at the 50-GeV PS.

For the double-spin asymmetry, a polarized hydrogen target is required. Technical progress concerning compact solid targets with less nuclear dilution is recently very rapid, and these technique will be adopted to the 50-GeV PS polarized target.

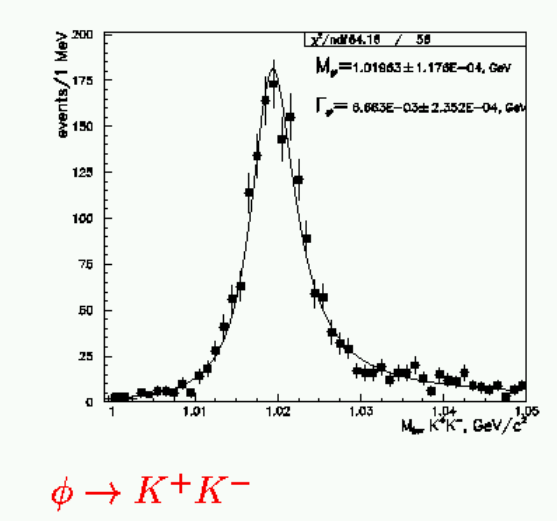

Figure 2.44: Mass distribution of ϕ.

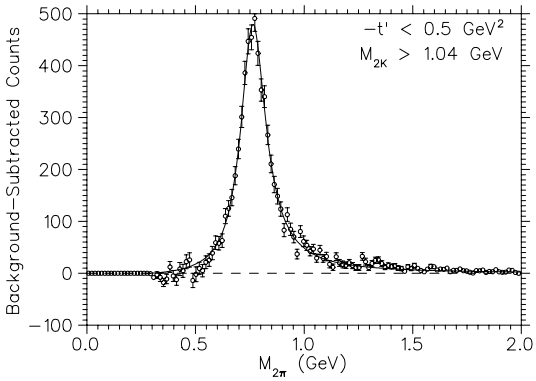

Figure 2.45: Mass distribution of ρ.

2.6.4 Summary

The spin asymmetry with a polarized proton beam on a proton target provides, when the meson and Λ productions are measured, information about the quark rearrangement, and particularly, how the spins of quarks and antiquarks become coupled. Analyses of these data will yield progress in our understanding and help to establish QCD in the non-perturbative region. Unlike analyses of the static properties of particles, we have parameters by which we can vary the reaction kinematics: large x_F, medium x_F region etc. This advantage can fully be used when we obtain a wide-acceptance hadron detector and record particle production over the full kinematic range with good particle identification. The polarized beam/target program at the 50-GeV PS will be a unique opportunity in the 50 GeV energy region.

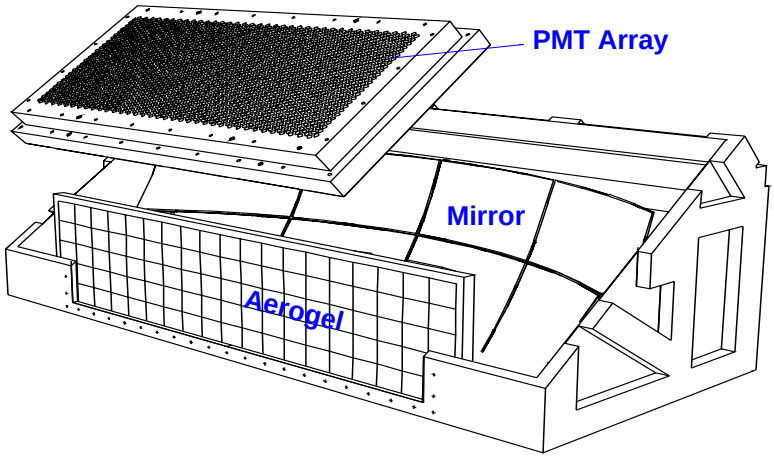

Figure 2.46: Overview of RICH of HERMES.

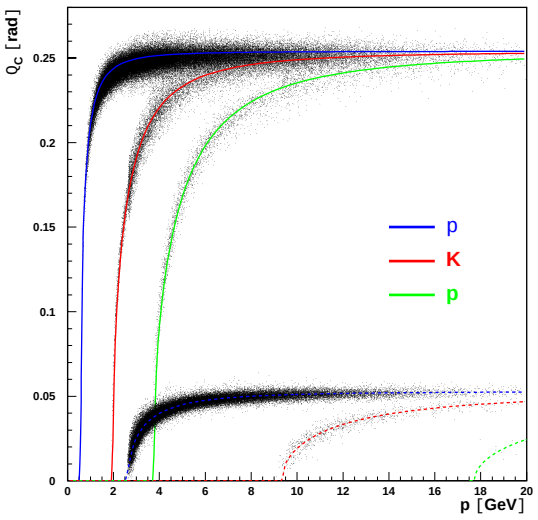

Figure 2.47: Cherenkof angle as a function of the momentum.

Chapter 3

Beam line

3.1 Introduction

We are planning several experiments to exploit the physics of strongly interacting many-body problems, as discussed in the previous chapter. Different type of beams are required for each experiment. In order to accommodate all or most of these experiments, the layout of the experimental area and beam lines must be carefully designed. We propose to construct a good-quality high-momentum beam line with which both primary and secondary beams can be transported.

3.2 Requirements for beams

In this section, the requirements for beams by the planned experiments are summarized as follows:

1. 50-GeV primary protons with an intensity of 10^{12} particles per second (pps)
   The muon-pair measurement requires a relatively high intensity beams to obtain a good sensitivity to the quark structure function at a large-x region. The beam intensity is limited to 10^{12} pps because of the background radiation level.

2. 50-GeV primary protons with an intensity of 10^{9} pps
   An experiment to study the vector meson properties in nuclear matter requires relatively low-intensity protons. The beam intensity is limited because its detector system is a two-arm spectrometer in an open geometry. The beam should be as clean as possible for the detector to work reasonably well: (1) the beam size should be as small as possible, less than 1mm in a diameter; (2) the beam position should be sufficiently stable, and (3) the beam halo should be as small as possible. Low-momentum (1$\sim$2 GeV/c) separated kaon and/or pion beams are very useful for detector calibrations.

3. 10^{9} pps 5$\sim$50 GeV variable-energy primary proton beam
   The multifragmentation experiment requires beams with variable energy. Variable energy is essential, because, so far, curious phenomena in the multifragmentation processes were observed in the excitation function. Requirements on the beam quality are the same as those for the previous beam type.

4. 10^{9} pps 5$\sim$30 GeV variable-energy secondary particle beams
   High-momentum secondary beams are required in several experiments which are not described in this article. For example, high-momentum π^- beams are essential for meson spectroscopy, high-momentum kaons may be used for productions of $S = -3$ hypernuclei, and high-momentum antiprotons may open the door to the production of charmed

hypernuclei. The beam line can also be used as a spectrometer in the search for exotic particles.

5. 10^{10} ions per second (ips) primary heavy-ion beam
   When light heavy-ions ($\sim$Ca) are accelerated at the 50-GeV PS, a new method becomes available for precision measurements of the magnetic moment of hypernuclei by producing them in the projectile region. Relatively high intensity (10^{10} ips) is necessary to obtain sufficient statistics. The separation between the beam and the relativistic Λ hypernulei is very small, even after passing through a strong magnetic field. Therefore, the beam spot size on the production target should be as small as possible, and the beam halo should not be there. The beam intensity could be moderate for other heavy-ion experiments, but the beam line must be designed to transport particles with variable energies. The beam line may also be used as a spectrometer to measure the particle productions of rare processes, or to search for exotic particles, as for proton beams.

3.3 Discussions

There are many different requirements for beams, as described in the previous section. We found a good solution to handle those requirements in a single beam line instead of making beam lines for each requirement. The solution is called a multi-purpose high-momentum beam line in which different beams can be transported by switching its most upstream part. By using a Lambertson magnet at the most upstream part, the primary 50 GeV protons with a moderate intensity (10^{12} pps) can be transported. For a small intensity ($\sim 10^9$ pps) of primary protons, the most upstream part is the "halo collector magnets" which is a specially designed Lambertson magnet and/or beam collimator made of magnetized iron. The halo collector can steal 1%$\sim$10ppm of the full primary proton beam. If the beam line is used for secondary beam transportation, the most upstream part is the production target. A realistic option to construct this multi-purpose beam line is to modify one of primary proton beam lines of the K arena. A possible location and configuration of this multi-purpose beam line is shown in Fig. 3.1.

It should be noted that the very high-intensity primary proton beam from the 50-GeV PS (10^{14}pps) will provide a "high intensity" secondary beam of up to $\sim 10^9$pps. Then, the multifragmentation experiment can enjoy a variable energy "primary" beam by using secondaries as incident particles. The highest momentum may be limited below 30$\sim$35 GeV/c. However, this "highest" momentum is high enough to cover the interesting energy region where many exotic phenomena occur as functions of the incident particle energy. The problem is the beam quality. It is almost impossible to prepare a pure proton beam at high momentum where the βs of all the secondaries are almost unity. However, if negatively charged particles can be used as the incident beam, it will be almost a pure π^- beam. A possible problem is the background μs decaying from πs. A separation problem may appear for the high momentum secondary kaon/antiproton users. An RF separator can work below $\sim$20 GeV/c. However, it is not practical to install an RF separator in the primary proton beam line. One option is to prepare a "low momentum (below $\sim$20 GeV/c)" branch beam line, as shown in Fig. 3.1.

It should also be noted that a long switchyard section is essential at the upstream part of the multi-purpose beam line. The initial beam purification, such as the emittance limitation and the halo rejection etc., will be performed at the "switchyard". One example is to install a "dogleg" section at the most upstream part. It must be remembered that the upstream part of the beam line is a highly radioactive area. It is very hard to make modifications there after the initial construction. The downstream part of the beam line can be modified later. It should also be remembered that the beam quality of the multi-purpose beam line is determined at the most upstream part. Therefore, special care should be given to the switchyard area.

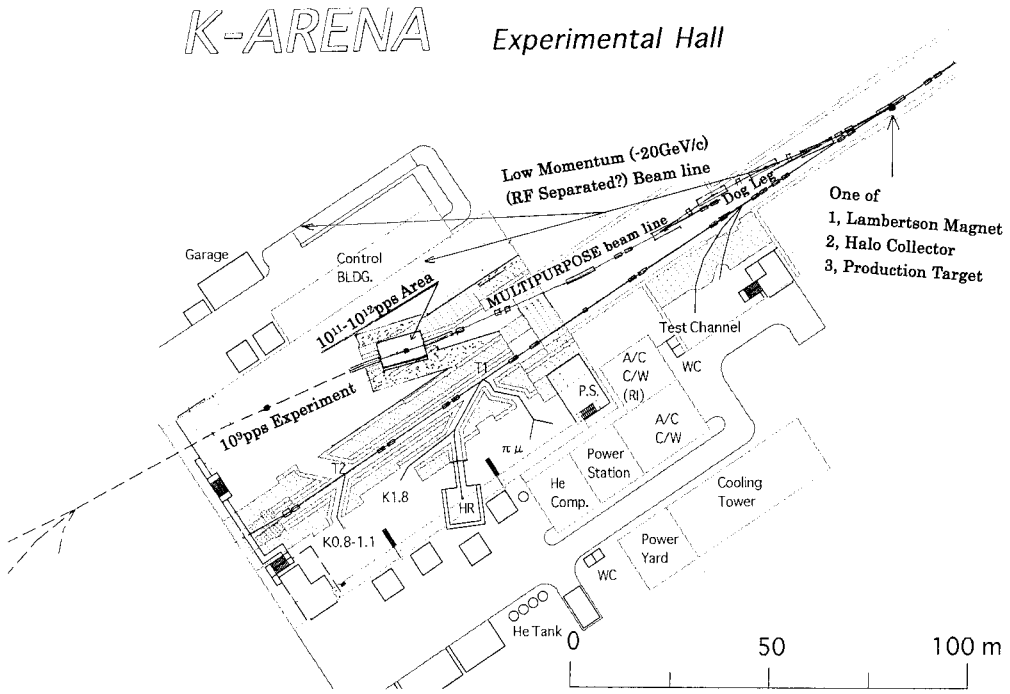

Figure 3.1: Location and configuration of the multipurpose beam line and its low momentum ($\sim$ 20GeV/c) branch.

The configuration of the experimental area is not yet fixed. At least two experimental points can be prepared on the multi-purpose beam line in cascade with the presently designed K-arena experimental hall. The experiments, which uses 10^{12} pps protons and 10^{10} ips heavy-ions, should be located at the most upstream experimental point where the radiation shield is relatively thick. An extra one or two experimental points can be prepared at the "RF-separated" branch line. A very natural extension for the extra experimental points is in the downstream direction. If an extension to the downstream direction might be forbidden because of the windbreak forest or the coastline, the extension should be in the sideward direction. In order to keep the possibility to extend the new experimental points to the sideward direction, we should be careful to prepare as long (and wide) a switchyard as possible. In addition, a permanent control building etc. should not be constructed at location of the possible extension direction of the K-arena experimental hall.

3.4 Conclusion

We would like to propose to construct a high-momentum beam line at the experimental hall of the 50-GeV PS. The beam line can be used for the transportation of both primary and secondary beams. The most upstream part of the beam line should be switched to the (1) Lambertson Magnet, (2)Halo Collector, and (3)Production Target. A realistic option to construct this beam line is to modify one of the primary beam lines for the K-arena. The beam line requires a long switchyard position upstream of the experimental area to provide a very good quality beam. A long (and wide) switchyard section is also essential to extend the beam line to the sideward

direction. One option is to construct an RF separated low-momentum ($\sim$20 GeV) beam line.

Chapter 4

Summary

In this article, we express our intention to pursue the rich and important but yet unsolved field of physics, that is, physics of strongly interacting many body problems, using various kinds of beams including the primary beam provided by the planned 50-GeV Proton Synchrotron at the KEK/JHF and JAERI/NSP joint accelerator project.

There are many possible scenarios and different approaches to exploit the physics of strongly interacting many body problems. The physics topics mentioned in this article certainly do not cover all of them, but might be one the best approaches.

The modification of the vector meson properties in nuclear matter is one of the most interesting topics in contemporary nuclear physics. Since this phenomenon might be the precursor to the restoration of spontaneously breaking chiral symmetry, extensive and systematic study may shed light on the phase transition of nuclear matter.

Measurements of the high-mass muon pairs give us various information through the Drell-Yan processes and vector meson productions. First of all, the muon-pair measurement at 50 GeV uniquely provides us information on the structure function of quarks in the large-x region. Anti u/d quark asymmetry and nuclear effects in the Drell-Yan processes are also interesting. Physics of heavy quarkonium is another interesting topics by which we can set constraints on the mechanism of vector meson productions. When polarized proton beam becomes available, polarization of sea quarks can be studied though which we can challenge the Spin Crisis problem. Polarized beam also provide us a chance to investigate the mechanism of quark-antiquark coupling to form a meson by measuring spin asymmetry.

Liquid-gas phase transition has been intensively studied by multiple productions of nuclear fragments, mainly using intermediate-energy heavy-ion reactions. High-energy nuclear reactions can also be used to study the phenomena. Measurements of multifragments in a range of wide incident energies give information on the equation of state (EOS).

Strangeness in nuclear matter is another interesing issue in contemporary nuclear physics. Production of hypernuclei in the projectile fragmentation region by heavy-ion collisions is a unique and useful method to invesigate the magnetic moment of Λ hypernuclei. Study of hypernulcei with the strangeness greater than 2 can be carried out only by heavy-ion reactions.

Once heavy ions are accelerated at the 50-GeV PS, another kind of phyics opens up. Since the beam energy is between those at BNL-AGS and at CERN-SPS, systematic and detailed studies of the collective flow become possible by which the conditions for the phase transition to the quark gluon plasma (QGP) phase might be studied.

In order to challenge the rich and important physics of strongly interacting many body problems, many different types of exmepriments should be carried out as described in this article. Of course, it is not necessary to perform them at the same time but as a series in order of suitable manner. Since the experimental hall planned at the moment is not large enough to accommodate two or more beamlines for the experiments mentioned in this article, we propose to

construct a multipurpose high-momentum beamline. The multipurpose beamline can transport the following beams; (1) 10^{12} particle per second (pps) primary beam, (2) 10^9 pps primary proton beam, (3) 10^9 pps $5 \sim 50 GeV$ variable energy proton beam, and (4) 10^9 pps $5 \sim 30 GeV$ variable energy secondary particle beam.

Bibliography

[1] D. J. Gross and F. Wilczek, Phys. Rev. Lett. **30** (1973) 1343.

[2] H. D. Polotzer, Phys. Rev. Lett. **30** (1973) 1346.

[3] See, e.g., D. Pines, *Elementary Excitations in Solids* (W.A. Benjamin, New York, 1963).

[4] T. Hatsuda and S. H. Lee, Phys. Rev. C **46** (1992) R34.

[5] T. Hatsuda, Y. Koike, and S. H. Lee, Nucl. Phys. **B394** (1993) 221.

[6] E. V. Shuryak, Rev. Mod. Phys. **65** (1993) 1.

[7] M. Asakawa, T. Hatsuda, and Y. Nakahara, to appear in Prog. Part. Nucl. Phys..

[8] L. D. Landau and I. J. Pomeranchuk, Dolk. Akad. Nauk. SSSR **92** (1953) 92.

[9] A. B. Migdal, Phys. Rev. **103** (1956) 1811.

[10] R. Baier, Yu. L. Dokshitzer, A. H. Mueller, S. Peigne, and D. Shiff, Nucl. Phys. B **484** (1997) 265.

[11] R. Baier, Yu. L. Dokshitzer, A. H. Mueller, and D. Shiff, Nucl. Phys. B **531** (1998) 403.

[12] B. G. Zhakharov, JETP Letters **63** (1996) 952.

[13] B. G. Zhakharov, JETP Letters **65** (1997) 615.

[14] M. Gyulassy, P. Lévai, and I. Vitev, nucl-th/0005032.

[15] L. Ahle et al. (the E866 Collaboration), Nucl. Phys. **A610** (1996) 139c.

[16] J. Bächler et al. (the NA49 Collaboration), Nucl. Phys. **A661** (1999) 45c.

[17] See, e.g., I. Montvay and G. Münster, *Quantum Fields on a Lattice* (Cambridge Univ. Press, Cambridge, 1994).

[18] E. Braaten and P. D. Pisarski, Nucl. Phys. **B337** (1990) 569.

[19] A. D. Linde, Phys. Lett. **B96** (1980) 289.

[20] D. J. Gross, R. D. Pisarski, and L. G. Yaffe, Rev. Mod. Phys. **53** (1981) 43.

[21] T. Hatsuda and T. Kunihiro, Phys. Rep. **247** (1994) 221.

[22] G. Brown and M. Rho, Phys. Rep. **269** (1996) 333.

[23] R. Rapp and J. Wambach, hep-ph/9909229 to appear in Adv. Nucl. Phys.

[24] G. Agakchiev *et al.*(CERES Collaboration), Phys. Lett. **B422** (1998) 405.

[25] T. Hatsuda and S. H. Lee, Phys. Rev. C **46** (1992) R24.

[26] G. Brown and M. Rho, Phys. Rev. Lett. **66** (1991) 2720.

[27] M. Asakawa, C.M. Ko, P. Levai and X. J. Qiu, Phys. Rev. C **46** (1992) 1159; M. Herrmann, B. Friman and W. Norenberg, Z. Phys. A **343** (1992) 119; G. Chanfray and P. Schuck, Nucl. Phys. A **545** (1992) 271c.

[28] K. Saito, K. Tsushima and A. W. Thomas, Phys. Rev. C **55** (1997) 2637.

[29] Proceedings of the International workshop XXVIII on Gross Properties of Nuclei and Nuclear Excitations (Hirschegg, Austria, Jan.16-22, 2000), ed. M. Buballa, W. Nörenberg, B. -J. Schaefer and J. Wambach.

[30] G. J. Lolos *et al.* (TAGX Collaboration), Phys. Rev. Lett. **80** (1998) 241.

[31] E325 proposal, http://www.pn.scphys.kyoto-u.ac.jp/~enyo/e325/phi_root.ps.Z; S. Yokkaichi, Memoir of The Faculty of Science, Kyoto University, (doctor thesis) in print.

[32] T. Kinashi, K. Takanashi, M. Fujiwara, T. Hotta, T. Nakano, In Hyogo 1997, Exciting physics with new accelerator facilities 55.

[33] W. Schoen *et al.* (HADES Collaboration), Acta Phys. Polon. B **27** (1996) 2959.

[34] GSI/SIS proposal S214, Search for bound η- and ω- nuclear states using the recoilless $(d,^3He)$ reaction.

[35] M. Binkley *et al.*, Phys. Rev. Lett. **37** (1976) 571.

[36] C. Daum *et al.*, Z. Phys. C **18** (1983) 1; R. Bailey *et al.*, Z. Phys. C **22** (1984) 125.

[37] A. N. Aleev *et al.*, JINR, D1-90-168 (1990), Dubna.

[38] T. Hatsuda, nucl-th/9702002, in Proceedings of the 25th INS International Symposium on Nuclear and Particle Physics with High-Intensity Proton Accelerators (Tokyo, Japan, 1997), ed. T. K. Komatsubara, T. Shibata and T. Nomura.

[39] J. J. Aubert *et al.*, Phys. Lett. **B123** (1983) 295.

[40] D. F. Geesaman, K. Saito, A. W. Thomas, Annu. Rev. Nucl. Part. Sci. **45** (1995) 337.

[41] E. Hughes and R. Voss, Annu. Rev. Nucl. Part. Sci. **49** (1999) 303.

[42] P. Amaudruz *et al.*, Phys. Rev. Lett. **66** (1991) 2712; M. Arneodo *et al.*, Phys. Rev. D **55** (1994) R1.

[43] K. Gottfried, Phys. Rev. Lett. **18** (1967) 1174.

[44] S. D. Drell and T. M. Yan, Phys. Rev. Lett. **25** (1971) 316 .

[45] P. L. McGaughey, J. M. Moss and J. C. Peng, Annu. Rev. Nucl. Part. Sci. **49** (1999) 217.

[46] E. A. Hawker *et al.*, Phys. Rev. Lett. **80** (1998) 3715.

[47] J. C. Peng *et al.*, Phys. Rev. D **58** (1998) 092004.

[48] D. A. Alde *et al.*, Phys. Rev. Lett. **64** (1990) 2479.

[49] D. I. Diakonov *et al.*, Phys. Rev. D **56** (1997) 4069.

[50] M. Wakamatsu and T. Kubota, Phys. Rev. D **60** (1999) 034020.

[51] R. Baier *et al.*, Phys. Lett. **B345** (1995) 277; Nucl. Phys. **B483** (1997) 291; Nucl. Phys. **B484** (1997) 265.

[52] R. G. Zakharov, JETP Letters **63** (1996) 952; JETP Letters **65** (1997) 615.

[53] L. D. Landau and I.Ya. Pomeranchuk, Dokl. Akad. Nauk SSSR **92** (1953) 535; **92** (1953) 735.

[54] A. B. Migdal, Phys. Rev. **103** (1956) 1811.

[55] P. L. Anthony *et al.*, Phys. Rev. Lett. **75** (1995) 1949; Phys. Rev. D **56** (1997) 1373.

[56] M. A. Vasiliev *et al.*, Phys. Rev. Lett. **83** (1999) 2304.

[57] J. C. Peng, hep-ph/9912371 (1999).

[58] C. Gerschel and J. Hüfner, Annu. Rev. Nucl. Part. Sci. **49** (1999) 255.

[59] R. Vogt, Phys. Rev. C **61** (2000) 035203.

[60] T. Matsui and H. Satz, Phys. Lett. **B178** (1986) 416.

[61] M. C. Abreu *et al.*, CERN-EP-2000-013 (2000).

[62] I. R. Kenyon, Rep. Prog. Phys. **45** (1982) 1261.

[63] J. Badier *et al.*, Z. Phys. C **26** (1984) 489.

[64] G. Moreno *et al.*, Phys. Rev. D **43** (1991) 2815.

[65] P. L. McGaughey *et al.*, Phys. Rev. D **50** (1994) 3038.

[66] H. L. Lai *et al.*, Phys. Rev. D **55** (1997) 1280.

[67] K. Freudenreich, Int. J. Mod. Phys. A **5** (1990) 3643.

[68] A. D. Martin *et al.*, Eur. Phys. J. C **4** (1998) 463.

[69] H. Abromowicz *et al.*, Z. Phys. C **15** (1982) 19.

[70] S. D. Ellis and W. J. Stirling, Phys. Lett. **B256** (1991) 258.

[71] P. L. McGaughey *et al.*, Phys. Rev. Lett. **69** (1991) 1726.

[72] A. Baldit *et al.*, Phys. Lett. **B332** (1994) 244.

[73] A. D. Martin, R. G. Roberts, W. J. Stirling, Phys. Lett. **B387** (1996) 419.

[74] A. W. Thomas, Phys. Lett. **B126** (1983) 97.

[75] J. D. Sullivan, Phys. Rev. D **5** (1972) 1732.

[76] S. Kumano, Phys. Rept. **303** (1998) 183.

[77] E. J. Eichten, I. Hinchliffe, C. Quigg, Phys. Rev. D **45** (1992) 2269.

[78] T. P. Cheng and L. F. Li, Phys. Rev. Lett. **74** (1995) 2872.

[79] A. Szczurek, A. Buchmans, A. Faessler, J. Phys. C **22** (1996) 1741.

[80] K. Ackerstaff et al., Phys. Rev. Lett. **81** (1998) 5519.

[81] S. Kumano, Phys. Rev. D **43** (1991) 3067; Phys. Rev. D **43** (1991) 59; S. Kumano and J. T. Londergan, Phys. Rev. D **44** (1991) 717.

[82] P. V. Pobylitsa *et al.*, Phys. Rev. D **59** (1999) 034024.

[83] A. A. Belavin et al., Phys. Lett. **B59** (1975) 85.

[84] G. t'Hooft, Phys. Rev. Lett. **37** (1976) 8.

[85] T. Schaefer and E. Shuryak, Rev. Mod. Phys. **70** (1998) 323.

[86] S. Forte, Phys. Lett. **B224** (1989) 189.

[87] S. Forte, Acta Phys. Polon. B **22** (1991) 1065.

[88] A. E. Dorokhov and N. I. Kochelev, Phys. Lett. **B259**, 335 (1991); **B335** (1993) 167.

[89] Proposal for Drell-Yan Measurements of Nucleon and Nuclear Structure with FNAL Main Injector, P906 Collaboration, http://p25ext.lanl.gov/e866/papers/p906/proposal_final.ps.

[90] B. Adeva *et al.*, Phys. Lett. **B420** (1998) 180.

[91] K. Ackerstaff *et al.*, hep-ex/9906035 (1999).

[92] B. Dressler *et al.*, hep-ph/9909541 (1999).

[93] R. J. Fries and A. Schäfer, Phys. Lett. **B443** (1998) 40.

[94] K. G. Boreskov and A. B. Kaidalov, Eur. Phys. J. C **10** (1999) 143.

[95] T. Gehrmann and W. J. Stirling, Phys. Rev. D **53** (1996) 6100.

[96] M. Glück, E. Reya, M. Stratmann and W. Vogelsang, Phys. Rev. D **53** (1996) 4775.

[97] K. Goeke *et al.*, hep-ph/0003324 (2000).

[98] M. Glück, E. Reya and A. Vogt, Z. Phys. C **67** (1995) 433.

[99] F. E. Close and D. Sivers, Phys. Rev. Lett. **39** (1977) 1116.

[100] D. Adams *et al.*, Nucl. Instru. Meth. **A437** (1999) 23.

[101] J. Ralston and D. E. Soper, Nucl. Phys. **B152** (1979) 109.

[102] R. L. Jaffe and X. Ji, Phys. Rev. Lett. **67** (1991) 552.

[103] S. Kumano, hep-ph/0001053 (2000).

[104] C. H. Llewellyn-Smith, Phys. Lett. **B128** (1983) 107.

[105] M. Ericson and A. W. Thomas, Phys. Lett. **B128** (1983) 112.

[106] E. L. Berger, F. Coester and R. B. Wiringa, Phys. Rev. D **29** (1984) 398.

[107] R. P. Bickerstaff *et al.*, Phys. Rev. Lett. **53** (1984) 2531.

[108] V. R. Pandharipande *et al.*, Phys. Rev. C **49** (1994) 789; A. Akmal *et al.*, Phys. Rev. C **56** (1997) 2261.

[109] F. E. Close, R. L. Jaffe, R. G. Roberts and G. G. Ross, Phys. Rev. D **31** (1985) 1004.

[110] R. Baier, D. Schiff and B. G. Zakharov, hep-ph/0002198 (2000).

[111] S. Gavin and J. Milana, Phys. Rev. Lett. **68** (1992) 1834.

[112] S. J. Brodsky and P. Hoyer, Phys. Lett. **B298** (1993) 165.

[113] M. H. Schub *et al.*, Phys. Rev. D **52** (1995) 1307.

[114] M. S. Kowitt *et al.*, Phys. Rev. Lett. **72** (1994) 1318.

[115] J. Pochodzalla *et al.*, Phys. Rev. Lett. **73** (1995) 1040.

[116] K. H. Tanaka *et al.*, Nucl. Phys. **A583** (1995) 581c.

[117] T. Murakami *et al.*, Perspectives in Heavy Ion Physics, ed. M. Ishihara *et al.*, (World Scientific, Singapore, 1996) 152.

[118] H. Ochiishi *et al.*, Nucl. Instr. and Methods **A369** (1996) 269.

[119] A. S. Hirsch *et al.*, Phys. Rev. C **29** (1984) 508.

[120] L. Schachinger *et al.*, Phys. Rev. Lett. **41** (1978) 1348.

[121] H. Bhang, *et. al*, Phys. Rev. Lett. **81** (1998) 4321.

[122] K.J. Nield *et al.*, Phys. Rev. **13** (1976) 1263.

[123] S.Avramenko *et al.*, Nucl. Phys. **A547** (1992) 95c.

[124] H. Bando, M. Sano, M. Wakai and J. Zofka, Nucl. Phys. **A501** (1989) 900.

[125] M. Sano and M. Wakai, Prog. Thor. Phys. Suppl. **117** (1994) 99.

[126] Nucl. Phys. **A625** (1997) 95.

[127] Y. Tanaka, Prog. Theeor. Phys. **82** (1989) 96, Phys. Lett. **B227** (1989) 195, Int. J. Mod. Phys. **E2** (1993) 423.

[128] T. Takeuchi, K. Shimizu, K. Nakai, Nucl. Phys. **A481** (1988) 693.

[129] M. Sano and M. Wakai, Prog. Theor. Phys. **100** (1998) 675.

[130] M. Wakai, private communication (2000).

[131] S. Chin and A. Kerman, Phys. Rev. Lett. **43** (1979) 1292.

[132] J. Barrette *et al.*, Phys. Lett. **B252** (1990) 550; A. Aoki *et al.*, Phys. Rev. Lett. **69** (1992) 2345; D. Beavis *et al.*, Phys Rev. C **54** (1996) R15; K. Borer *et al.*, Phys. Rev. Lett. **72** (1994) 1415; J. L. Nagel *et al.*, Nucl. Phys. **A661** (1999) 185c.

[133] K. Heller *et al.*, Phys. Rev. Lett. **41** (1978) 607.

[134] J. W. Harris *et al.*, Phys. Rev. Lett. **47** (1981) 229.

[135] L. Schachinger, *et al.*, Phys. Rev. Lett.**41** (1978) 1348; A. Morelos, *et al.*, Phys. Rev. Lett. **71** (1993) 3417; L. H. Trost, *et al.*, Phys. Rev. D **40** (1989) 1703.

[136] I. G. Bearden *et al.*, Phys. Rev. Lett. **78** (1997) 2080; I. G. Bearden *et al.*, Phys. Lett. **B388** (1996) 431; H. Boggild *et al.*, Z. Phys. C **69** (1996) 621; H. Beker *et al.*, Phys. Rev. Lett. **74** (1995) 3340.

[137] WA98 Collaboration, M. Kurata, *et al.*, Prog. Theor. Phys. Suppl. **129** (1997) 179; B. Wyslouch *et al.*, Nucl. Phys. **A638** (1998) 147c; S. Nishimura *et al.*, Nucl. Phys. **A638** (1998) 459c; M. M. Aggarwal *et al.*, Nucl-ex/9807004.

[138] M. M. Aggarwal *et al.*, Phys.Lett. **B469** (1999) 30.

[139] M. C. Abreu *et al.*, Phys. Lett. **B477** (2000) 28; M. C. Abreu *et al.*, Phys. Lett. **B450** (1999) 456.

[140] G. Agakichiev *et al.*, Phys. Lett. **B422** (1998) 405; G. Agakichiev *et al.*, Nucl. Phys. **A638** (1998) 159c.

[141] F. Antinori *et al.*, Nucl. Phys. **A661** (1999) 130c.

[142] H. Stöcker and W. Greiner, Phys. Rep. **137** (1986) 277.

[143] D. H. Rischke, Nucl. Phys. **A610** (1996) 88c .

[144] J. -Y. Ollitrault, Phys. Rev. D **46** (1992) 229; J. -Y. Ollitrault, Phys. Rev. D **48** (1993) 1132; J. -Y. Ollitrault, Nucl. Phys. **A638** (1998) 195c.

[145] C. M. Hung and E. V. Shuryak, Phys. Rev. Lett. **75** (1995) 4003.

[146] NA49 Collaboration, T. Wienold *et al.*, Nucl. Phys. **A610** (1996) 76c; H. Appelshäuser *et al.*, Phys. Rev. Lett. **80** (1998) 4136; A. M. Poskanzer *et al.*, Nucl. Phys. **A638** (1998) 463c.

[147] G. Q. Li and C. M. Ko, Nucl. Phys. **A594** (1995) 460; G. Q. Li, C. M. Ko and B. A. Li, Phys. Rev. Lett. **74** (1995) 235.

[148] K. Enosawa, Doctor thesis at University of Tsukuba.

[149] P. Braun-Munzinger *et al.,*, Phys. Lett. **B465** (1999) 15.

[150] T. Chujo, Doctor thesis at University of Tsukuba.

[151] U. Heinz *et al.,* Phys.Lett. **B382** (1986) 181.

[152] H. Appelshauser *et al.,*, Eur. Phys. J. C **2** (1998) 661.